Techniques for Improving Li-Fi Data Rate for Display Systems with Visible Light Communication Capability

by

Liusheng SUN

A Thesis Submitted to
the Hong Kong University of Science and Technology
in Partial Fulfillment of the Requirements for
the Degree of Master of Philosophy
in the Department of Electronic and Computer Engineering

October 2017, Hong Kong

Authorization

I hereby declare that I am the sole author of the thesis.

I authorize the Hong Kong University of Science and Technology to lend this thesis to other institutions or individuals for the purpose of scholarly research.

I further authorize the Hong Kong University of Science and Technology to reproduce the thesis by photocopying or by other means, in total or in part, at the request of other institutions or individuals for the purpose of scholarly research.

Liusheng Sun

Liusheng SUN

October 2017

Techniques for Improving Li-Fi Data Rate for Display Systems with Visible Light Communication Capability

by

Liusheng SUN

This is to certify that I have examined the above MPhil thesis and have found that it is complete and satisfactory in all respects, and that any and all revisions required by the thesis examination committee have been made.

Prof. C. Patrick YUE, ECE Department (Thesis Supervisor)

Prof. Bertram SHI (Head of ECE Department)

Thesis Examination Committee:

- 1. Prof. Ross MURCH (Chairperson), Department of Electronic and Computer Engineering
- 2. Prof. C. Patrick YUE (Supervisor), Department of Electronic and Computer Engineering
- 3. Prof. Danny Hin Kwok TSANG, Department of Electronic and Computer Engineering

Department of Electronic and Computer Engineering
The Hong Kong University of Science and Technology
October 2017

To my family

Acknowledgements

First and foremost, I would like to give my greatest thanks to my supervisor, Prof. Patrick Yue, for the insightful guidance, great encouragement, and kind support during my MPhil study. He offered me a great opportunity to work on this interesting and promising project. He shared wonderful ideas with me and provided timely advice to lead me on the right track of my research. Under his supervision, I learned extremely valuable lessons and skills that will continue to help me in my future endeavors.

I am also very thankful to Prof. Ross Murch and Prof. Danny Hin-Kwok Tsang for being my thesis committee members. I really appreciate their worthy time and their valuable comments and suggestions to help me improve my thesis.

I would also like to express my thanks to Dr. Xianbo Li and Mr. Babar Hussain for their technical help and guidance on numerous occasions.

My gratitude goes to Dr. Junmin Jiang and Mr. Xu Zhang for their respective contributions to the micro-display project. I was very fortunate to have them working with me on the same project. The experience benefits me greatly.

I want to thank Ms. Tania Wilmshurst as well for her enthusiastic help and support with my English in the thesis.

Additionally, I am thankful to my colleagues, both in and outside of my research group, , Dr. Haikun Jia, Dr. Yipeng Wang, Mr. Duona Luo, Mr. Guang Zhu, Mr. Zhixin Li, Mr. Li Wang, Mr. Shing Hin Yuen, etc. for extending their technical support whenever needed and being wonderful friends.

Last but not least, I would like to express my heartfelt thanks to my family for their unconditional love and support.

Table of Contents

Title Page
Authorizationii
Signature Pageiii
Acknowledgementsv
Abstractxi
CHAPTER 1 Introduction
1.1 Introduction to Visible Light Communication
1.2 VLC Systems with Different Light Sources
1.2.1 LED-based VLC4
1.2.2 LD-based VLC6
1.3 Micro-display Systems in Near-field Communication (NFC) Applications
1.4 Thesis Organization
References
CHAPTER 2 Adaptive Threshold Decoding Algorithms
2.1 Simultaneous Display and VLC Overview
2.1.1 Simultaneous Illumination and VLC (SI-VLC) and Simultaneous Display and
VLC (SD-VLC) Systems
2.1.2 Transmitted Optical Power Difference in SI-VLC and SD-VLC systems 12
2.2 Challenges in Data Recovery from Simultaneous Display and VLC systems 14
2.3 Proposed Adaptive Threshold Decision Algorithms
2.3.1 Preamble-based ATD Algorithm
2.3.2 Section-based ATD Algorithm
2.4 Experiments and Results
2.4.1 Experiment Setup
2.4.2 Results and Discussion

Referer	ices		25		
CHAP	ΓER 3	Micro-display System with Visible Light Communication Capability	26		
3.1	AM	ALED Micro-display System Overview	27		
3.2	Fea	atures of Micro-LEDs	28		
3.2	2.1	I-V Characteristics of Micro-LEDs.	30		
3.2	2.2	C-V Characteristics of Micro-LEDs	30		
3.2	2.3	First Order Equivalent Circuit	32		
3.3	CM	MOS AMLED Driver	33		
3.3	3.1	Design and Timing of Row Driver	33		
3.3	3.2	Design and Timing of Column Driver	35		
3.4	Pix	rel Driver	37		
3.4	4.1	Timing of Pixel Driver Array	39		
3.4	4.2	Conventional Mode Pixel Driver	41		
3.4	4.3	Proposed 2-Driving-Transistor Mode Pixel Driver	42		
3.5	Ex	periments and Results	44		
Referer	nces		47		
CHAP	ΓER [∠]	4 Conclusion and Future Work	48		
4.1	Co	nclusion	48		
4.2	4.2 Future Work				
Publica	tions		50		

List of Figures

Figure 1.1 Electromagnetic spectrum2
Figure 1.2 VLC systems using different LEDs: illumination, signage and display
Figure 1.3 Indoor illumination system integrated with VLC techniques [1.3]4
Figure 1.4 Apple device communicates with a POS reader through NFC [1.23]
Figure 2.1 (a) A generic simultaneous illumination and VLC (SI-VLC) system, (b) a generic
simultaneous display and VLC (SD-VLC) system
Figure 2.2 (a) Received VLC signal, (b) 4-bit PWM frame structure, (c) VLC data packets.
Figure 2.3 Amplitude variation in received signal due to continuously updating frames 15
Figure 2.4 Flow chart of the proposed Preamble-based Adaptive Threshold Decision
algorithm, (a) received signal sample, (b) set trigger level for recognition, (c) recognized VLC-
enabled periods, (d) calculated threshold values from Preamble-based ATD, (e) eye diagram
with a calculated threshold voltage of 1.79 V, (f) recovered VLC data
Figure 2.5 Received VLC signal with thresholds from Preamble-based and Section-based
ATD algorithms
Figure 2.6 Block diagram of simultaneous display and VLC experimental setup 20
Figure 2.7 (a) BER vs. normalized lit up pixels at 10 cm distance, (b) BER vs. distance. 21
Figure 3.1 System architecture of proposed AMLED micro-display system27
Figure 3.2 (a) Micrograph of micro-LED array, (b) cross sectional diagram of the micro-
LED array with indium bumps, (c) SEM of micro-LED array with indium bumps after reflow
process
Figure 3.3 Measured I–V characteristics of Micro-LEDs
Figure 3.4 Measured C–V characteristics of micro-LEDs
Figure 3.5 First-order equivalent circuit of the micro-LED.
Figure 3.6 Diagram of row driver
Figure 3.7 Timing of row driver
Figure 3.8 Diagram of column driver
Figure 3.9 Timing of column driver
Figure 3.10 (a) Proposed pixel driver can operate in different modes by $S_{\rm EN}$ settings, (b)
S _{EN} ='0', conventional mode, (c) S _{EN} ='1', proposed 2-driving-transistor mode
Figure 3.11 Structure of pixel driver array.
Figure 3.12 Timing of display data update

Figure 3.13 (a) Conventional mode pixel driver with '0' stored in C_{ST} and D_{VLC} input, (b)
when D_{VLC} ='0', forward current i_{LED} charges the micro-LED, (c) when D_{VLC} ='1', leakage
current i_{LK} flows through the micro-LED
Figure 3.14 (a) 2DT mode pixel driver with '0' stored in C _{ST} and D _{VLC} input, (b) when
D_{VLC} ='0', forward current i_{LED} charges the micro-LED, (c) when D_{VLC} ='1', power supply
VEXT sinks the current i_s from C_p , (d) current i_h from VEXT compensates for the leakage
current i_{LK} and maintains the value of V_{LED}
Figure 3.15 VLC experimental setup
Figure 3.16 BER vs. data rate of conventional and 2DT mode pixel driver at 10 cm distance,
(a) with 20 μA per pixel, (b) with 30 μA per pixel
Figure 3.17 BER vs. distance of 2DT mode driver with 30 µA per pixel at 20 Mb/s data rate.
46

List of Tables

Table 2.1 VLC BER Comparison for AMLED Micro-Display System with 4-frame/s.	22
Table 2.2 BER Difference for Still Image and 4-frame/s Video	23

Techniques for Improving Li-Fi Data Rate for Display Systems with Visible Light Communication Capability

by

Liusheng SUN

Department of Electronic and Computer Engineering
The Hong Kong University of Science and Technology

Abstract

Visible light communication (VLC) using LEDs has recently attracted a great deal of research interest in Light-Fidelity (Li-Fi) applications. Previous studies mainly focus on the applications of simultaneous illumination and VLC. However, there are many LED-based displays, including LCD displays with LED backlights, OLED displays, and micro-LED displays, which can be exploited for the deployment of VLC using LEDs as transmitters. This thesis presents two decoding algorithms for Li-Fi data recovery and a VLC transmitter system-on-chip (SoC) with bandwidth improving techniques, focusing on simultaneous display and VLC applications.

The main challenge of VLC data recovery from a display is the varying received signal strength caused by changes in the displayed images or videos. This work proposes two Adaptive Threshold Decoding (ATD) algorithms which dynamically adjust the decision threshold voltage: Preamble-based ATD, utilizing the preamble sequence, and Section-based ATD, utilizing the characteristics of OOK modulation and Manchester encoding. The measured BER of a 4-frame/s micro-LED display is improved from 6.9×10^{-2} to 4.4×10^{-4} using the Preamble-based ATD algorithm compared with the conventional Constant Threshold Decision scheme, which is further improved to 3.6×10^{-4} by using Section-based ATD.

The proposed transmitter SoC is a second-generation active matrix light-emitting diode (AMLED) micro-display driver, simultaneously supporting display and VLC. The AMLED driver, consisting of a row driver, a column driver and proposed micro-LED pixel drivers, is flip-chip bonded with a blue gallium nitride (GaN) micro-LED array with 36×64 pixels, each measuring $40\times40~\mu\text{m}^2$. Implemented in a $0.18-\mu\text{m}$ CMOS process, the AMLED micro-display with the proposed pixel driver can achieve a 20-Mb/s bit rate at 10~cm without a lens, which is four times as large as the 5-Mb/s modulation bit rate in the first generation.

CHAPTER 1 INTRODUCTION

1.1 Introduction to Visible Light Communication

With the help of radio frequency (RF) wireless technologies, smart terminals, especially smartphones, have developed hugely in the last decade. At the same time, the consumer demand for data traffic is constantly increasing due to various multimedia applications. However, the radio spectrum, which is the frequency range from 3 kHz to 300 GHz, is becoming increasingly congested [1.1]. Hence the remaining RF spectrum is dwindling, and spectral management is becoming a concern [1.2]. Moreover, expensive licensing fees are charged by the government for usage of the RF frequency band. These factors are driving the need for an alternative technology [1.3].

Figure 1.1 shows the electromagnetic spectrum covering radio waves through to gamma rays. Along the electromagnetic spectrum, the frequency and energy of the waves increase as the wavelength decreases. Optical wireless communication, utilizing the unregulated optical spectrum above 300 GHz, is attractive as one of the solutions to overcome the crowded radio spectrum for wireless communications, as a supplement to RF wireless technologies. In addition, for energy saving reasons, light-emitting diodes (LEDs) are being deployed more and more ubiquitously to replace conventional incandescent and fluorescent lights. LEDs are able to be switched on and off rapidly to modulate light intensity for information delivery due to their inherent fast response compared to fluorescent lights. This switching speed or modulation frequency is far beyond the flicker fusion threshold of human beings, which means it won't affect illumination or display functions. Therefore, LEDs can be utilized as transmitters in visible light communication (VLC).

VLC is an optical wireless communication variant which utilizes visible light as the communication medium at wavelengths ranging from 380 nm to 780 nm [1.1] or frequencies between 400 THz and 800 THz (as shown in Figure 1.1). Generally, intensity modulation (IM) and direct detection (DD) are used in VLC systems on the transmitter and receiver side respectively for low complexity. Compared with conventional optical wireless communication modes, like infrared (IR) and ultra violet (UV), on the application level, the most distinguished feature of VLC is that it can utilize existing LEDs to support illumination and communication simultaneously.

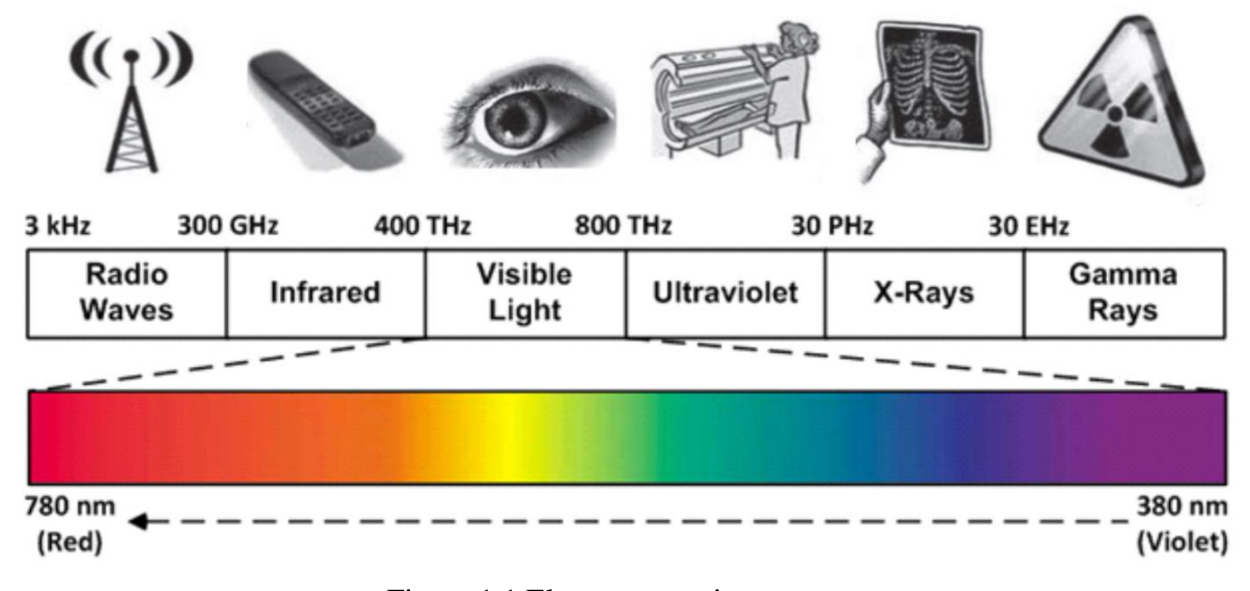


Figure 1.1 Electromagnetic spectrum.

In particular, a Light-Fidelity (Li-Fi) system can be formed by networking various VLC transceivers as a complete wireless system to support bi-directional multiuser communication with point-to-point, point-to-multipoint and multipoint-to-point communication techniques [1.4]. In other words, Li-Fi is a VLC networking system.

Compared with conventional RF communications, VLC utilizes the visible light emitted from illumination LEDs as the communication medium to concurrently transmit information through the line-of-sight (LOS) channel, and it has many advantages, listed as follows.

- (1) Unlicensed spectrum: Use of the RF spectrum has been assigned by administrative licensing since the 1930s, mainly to ensure efficient utilization and high communication quality. However, as mentioned above, the RF spectrum is becoming crowded due to the increasing data traffic demand from multimedia communications, cloud computation and other emerging applications. Visible light can be easily confined to a well-defined area surrounded by opaque boundaries due to its intrinsic LOS characteristics. And the visible light spectrum is available without licensing regulation, which is suitable for low-cost applications.
- (2) High bandwidth capacity: Radio waves correspond to a frequency band of ~3 kHz to ~300 GHz, while visible light corresponds to a frequency band of ~400 THz to ~780 THz. Thus, the visible light spectrum is 1000 times wider than that of radio waves [1.5], which provides the potential to support high data rates.

- (3) No electromagnetic-interference (EMI) with existing RF systems: Due to the larger frequency difference between visible light and radio waves, VLC does not cause any electromagnetic-interference (EMI) with existing RF communication systems and other EMsensitive systems [1.6]. Thus VLC is suitable to be deployed in places where radio wireless is not feasible, such as hospitals and airplanes [1.7]. In particular, hybrid systems that employ VLC and RF can achieve better performance by taking advantage of the merits of each technology [1.8–1.11]. For example, VLC can supplement conventional RF systems to give higher throughput and a larger coverage area, while RF can provide the uplink transmission capability for VLC systems to implement two-way communication.
- (4) Compliant with existing infrastructure: VLC can be implemented into existing lighting infrastructure with the addition of other blocks, such as a front-end and baseband [1.12]. Infrastructure-based VLC transmitters are widely deployed due to their symbiotic relationship with indoor energy efficient lighting [1.7]. With 12 billion light bulbs in operation around the world with unlicensed bandwidth, there can be 12 billion potential VLC transmitters [1.3].
- (5) Security: Unlike the radio waves in Wi-Fi, visible light cannot penetrate walls, which provides enhanced security in a well-defined space by avoiding interception.

1.2 VLC Systems with Different Light Sources

As mentioned in Section 1.1, one of the advantages of VLC is that existing light sources such as LEDs, whether used for illumination, signaling or display, can be 'reused' as transmitters to achieve an additional communication function, as shown in Figure 1.2. The light sources for VLC can be classified into two broad categories: LEDs, including micro-LEDs and ordinary commercial LEDs, and visible light laser diodes (LDs). In LD-based VLC, the modulated light from the laser is directed. Based on the different light sources, there are various applications of VLC, in which the modulated visible light data rate is ranging from megabit-per-second to gigabit-per-second. LED-based VLC can be further classified into simultaneous illumination and VLC (SI-VLC) applications, and simultaneous display and VLC (SD-VLC) applications. Most previous studies have focused on the former, while this thesis is about the latter.

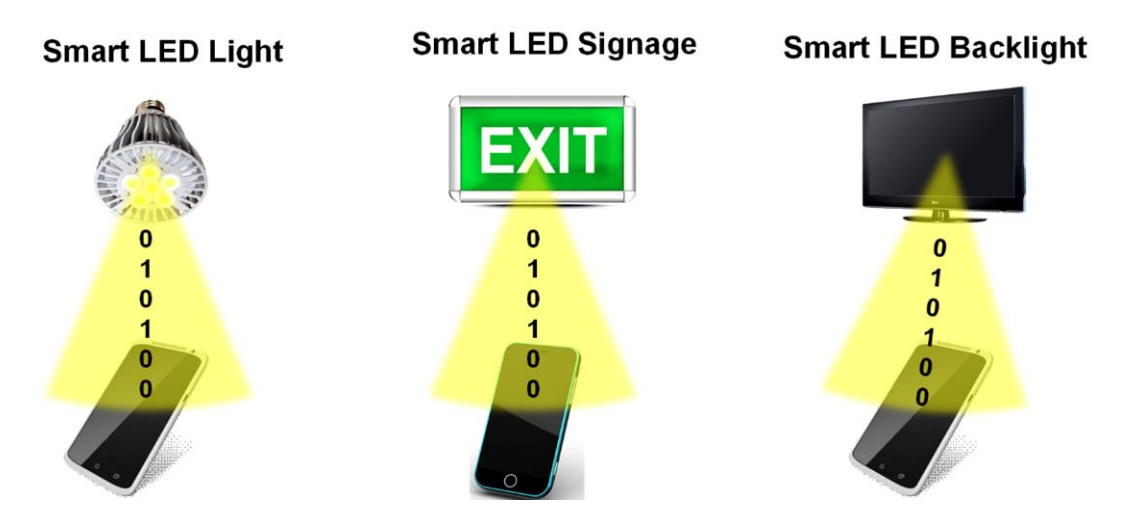


Figure 1.2 VLC systems using different LEDs: illumination, signage and display.

1.2.1 LED-based VLC

1. Simultaneous Illumination and VLC (SI-VLC). The situation of SI-VLC, which combines illumination and communication functions, is usually indoors. Figure 1.3 depicts the scenario that household devices are connected by a VLC-based wireless sensor network (WSN) for communication, monitoring and control [1.3]. SI-VLC systems, in which LEDs are used for simultaneous illumination and communication, can act as wireless data access points (APs), like the Wi-Fi hotspots in RF communications. And laptops, desktops and televisions can be connected to the Internet through the APs.



Figure 1.3 Indoor illumination system integrated with VLC techniques [1.3].

OOK modulation is extensively adopted in VLC due to the low complexity on the transmitter and receiver side. However, the bandwidth of commercial LEDs is usually around several megahertz. In 2008, multiple-resonant pre-equalization was employed to extend the -3 dB bandwidth of a white LED to 45 MHz and achieve an 80 Mb/s data rate with 10 cm distance by OOK modulation [1.13]. In 2014, an OOK VLC system based on a phosphorescent LED was reported to increase the -3 dB modulation bandwidth to 233 MHz, and achieve a 550 Mb/s data rate with a distance of 60 cm, by using both pre-equalization and postequalization circuits [1.14]. Furthermore, advanced modulation schemes have also been exploited for VLC applications. In 2010, a white LED based VLC link was able to achieve a 100 Mb/s data rate over a distance of 1.4 m, by using DMT modulation [1.15]. In 2012, rateadaptive DMT modulation for VLC was proposed to achieve data rates up to 1 Gb/s over 15 cm using a phosphorescent white LED [1.16]. In 2013, MIMO-OFDM was employed to enable 4-channel VLC transmission at a 1 Gb/s data rate using four phosphorescent white LEDs over a distance of 1 m [1.17]. In 2014, a VLC link involving 12 LEDs with four different colors (red, green, blue and amber) and WDM-OFDM modulation could support communication data rates as high as 5.6 Gb/s at a distance of 1.5 m [1.18]. In these systems, though using phosphorescent white LEDs, blue filters were utilized for bandwidth extension, and lenses were also adopted to strengthen the received signal.

2. Simultaneous Display and VLC (SD-VLC). Most previous studies introduced above have focused on SI-VLC applications. However, LEDs are widely used in many other applications, such as display applications. And nowadays, LED-based display systems, including LCD displays with LED backlights, OLED displays, and micro-LED displays, are also ubiquitous and can be exploited for VLC, with the LEDs acting as transmitters. The first active matrix LED (AMLED) micro-display with an embedded VLC transmitter was reported in [1.19]. The driver system-on-chip (SoC) drives a wide quarter-VGA display with 400×240 pixels of 30×30 μm² blue gallium nitride (GaN) micro-LEDs, simultaneously supporting 4-bit grayscale image display and VLC at a data rate of 1.25 Mb/s [1.19]. However, on the receiver side, the data recovery of VLC signals from the display presents additional design difficulties compared to lighting-based VLC systems. The main challenge is the varying received signal strength caused by the changes in the displayed images or videos. Hence the conventional constant threshold decoding scheme cannot handle it.

1.2.2 LD-based VLC

Compared with LEDs, LDs can operate at a higher current density, enabling a larger intrinsic bandwidth for high-speed optical communication. In 2015, a VLC system using a GaN 450 nm LD was reported to achieve a 4 Gb/s data rate at 15 cm distance with OOK modulation [1.20]. Another GaN 450 nm LD with a 1.5 GHz bandwidth was employed to achieve 9 Gb/s communication over a 5 m free-space link using 64-QAM OFDM in [1.21]. In 2016, 2.5 Gb/s OOK modulation was implemented over a 12 m distance via a 680 nm 5 GHz bandwidth LD [1.22]. Optical components such as lenses were employed in these systems to focus the transmitted light onto the receiver. However, LD-based VLC cannot support illumination and communication simultaneously.

1.3 Micro-display Systems in Near-field Communication (NFC) Applications

Those LED-based display systems with large size screen (over several tens of inches), which are widely used in both indoor and outdoor, such as shopping malls and squares, can be used as transmitters to achieve simultaneous display and VLC at several meter communication distance.

The communication distance of micro-display systems is around 10 cm, making it suitable for near-field communication (NFC) applications, especially for mobile payments. Nowadays, mobile payments like Apple Pay, in which payment services are performed via a mobile device, is getting more and more popular. A consumer can pay for services, digital or hard goods, using a mobile phone, instead of cash, check or credit cards. And NFC is one of the widely used methods in mobile payments, especially for purchases made in physical stores. For example, in Apple Pay, Apple devices wirelessly communicate with point of sale (POS) readers through NFC, as shown in Figure 1.4. And the distance for NFC is only several centimeters, which is designed to confine the communication in a limited space. However, for RF-based NFC technologies, security attacks, including eavesdropping the stored credit card information and other private information, maybe happen, even the communication distance is limited.



Figure 1.4 Apple device communicates with a POS reader through NFC [1.23].

Due to the short communication distance and higher directivity of the micro-LED compared with the antenna used in RF-based NFC, micro-display systems with VLC capability can confine the communication between POS readers and mobile devices in a well-defined space, which providing enhanced security. Nowadays, most POS readers are able to display some information during the payment with monochrome or color displays. And VLC can be implemented into the existing POS readers to achieve an additional communication function. Furthermore, due to the line-of-sight channel in VLC, it's easy to protect private information from security attacks just putting the devices into the pockets.

Thus, micro-display systems, supporting simultaneous display and VLC, can be used in POS readers for mobile payment applications and provide enhanced security, compared with other RF-based NFC technologies.

1.4 Thesis Organization

The rest of the thesis is organized as follows. In Chapter 2, the features of simultaneous display and VLC (SD-VLC) systems are introduced and compared with simultaneous illumination and VLC (SI-VLC) systems. Then the challenges in data recovery from SD-VLC on the receiver side are summarized, and adaptive threshold algorithms are proposed and verified experimentally. Chapter 3 describes the features of micro-LEDs and the design of a micro-display system with visible light communication capability. The proposed micro-LED driver with bandwidth extension techniques is verified by measurement results. Finally, the thesis is concluded and the future work is introduced in Chapter 4.

References

- [1.1] M. Oh, "A flicker mitigation modulation scheme for visible light communications," in *Proc. 15th ICACT*, PyeongChang, Korea, 2013, pp. 933–936.
- [1.2] B. Love, D. Love, and J. Krogmeier, "Like deck chairs on the titanic: Why spectrum reallocation won't avert the coming data crunch but technology might keep the wireless industry afloat," *Washington Univ. Law Rev.*, vol. 89, p. 705, 2012.
- [1.3] D. Karunatilaka, F. Zafar, V. Kalavally, and R. Parthiban. "LED Based Indoor Visible Light Communications: State of the Art." *IEEE communications surveys and tutorials* 17, no. 3 (2015): 1649-1678.
- [1.4] H. Haas *et al.*, "What is LiFi?" *IEEE J. Lightw. Technol.*, vol. 34, no. 6, pp. 1533–1544, Mar. 2016.
- [1.5] H. Parikh, J. Chokshi, N. Gala, and T. Biradar, "Wirelessly transmitting a grayscale image using visible light," in *Proc. ICATE*, Mumbai, India, 2013, pp. 1–6.
- [1.6] S. Zhao, J. Xu, and O. Trescases, "A dimmable LED driver for Visible Light Communication (VLC) based on llc resonant DC-DC converter operating in burst mode," in *Proc. 28th Annu. IEEE APEC Expo.*, LongBeach, CA, USA, 2013, pp. 2144–2150.
- [1.7] H. Ma, L. Lampe, and S. Hranilovic, "Integration of indoor visible light and power line communication systems," in *Proc. 17th IEEE ISPLC Appl.*, Johannesburg, South Africa, 2013, pp. 291–296.
- [1.8] M. Kashef, *et al.*, "Energy efficient resource allocation for mixed RF/VLC heterogeneous wireless networks," *IEEE Journal on Selected Areas in Communications*, vol. 34, no. 4, pp. 883-893, Apr. 2016.
- [1.9] D. A. Basnayaka, H. Haas, "Design and analysis of a hybrid radio frequency and visible light communication system," *IEEE Transactions on Communications*, no. 99, pp. 1-1, 2017.
- [1.10] X. Li *et al.*, "Cooperative load balancing in hybrid visible light communications and WiFi," *IEEE Transactions on Communications*, vol. 63, no. 4, pp. 1319-1329, Apr. 2015.
- [1.11] Y. Wang, H. Haas, "Dynamic load balancing with handover in hybrid Li-Fi and Wi-Fi networks," *IEEE Journal of Lightwave Technology*, vol. 33, no. 22, pp. 4671-4682, Nov. 2015.
- [1.12] A. Jovicic, J. Li, and T. Richardson, "Visible light communication: opportunities, hallenges and the path to market," *IEEE Commun. Mag.*, vol. 51, no. 12, pp. 26–32, Dec. 2013.
- [1.13] H. Le-Minh, D. O'Brien, G. Faulkner, *et al.*, "80 Mbit/s visible light communications using pre-equalized white LED," *European Conference on Optical Communication (ECOC)*, pp. 1–2, 2008.

- [1.14] H. Li, *et al.*, "A 550 Mbit/s real-time visible light communication system based on phosphorescent white light LED for practical high-speed low complexity application," *Opt Express*, vol. 22, no. 22, pp. 27203-27213, 2014.
- [1.15] J. Vucic, L. Fernandez, C. Kottke, K. Habel, and K.-D. Langer. "Implementation of a Real-Time DMT-Based 100 Mbit/s Visible-Light Link", in *36th European. Conference and Exhibition on Optical Communication*, pp. 1–5, September 2010.
- [1.16] A. M. Khalid, G. Cossu *et al.*, "1-Gb/s Transmission Over a Phosphorescent White LED by Using Rate-Adaptive Discrete Multitone Modulation," *IEEE Photonics Journal*, vol. 4, no. 5, pp. 1465–1473, Oct. 2012.
- [1.17] A. H. Azhar, T. A. Tran, D. O'brien, "A gigabit/s indoor wireless transmission using MIMO-OFDM visible-light communications," *IEEE Photonics Technol. Lett.*, vol. 25, no. 2, pp. 171-174, 2013.
- [1.18] G. Cossu, *et al.*, "5.6 Gbit/s downlink and 1.5 Gbit/s uplink optical wireless transmission at indoor distances (≥1.5 m)," *European Conference on Optical Communication (ECOC)*, 2014.
- [1.19] X. Li, et al., "Design and characterization of active matrix led microdisplays with embedded visible light communication transmitter." *Journal of Lightwave Technology*, 2016.
- [1.20] C. Lee *et al.*, "4 Gbps direct modulation of 450 nm GaN laser for high-speed visible light communication," *Opt. Express*, vol. 23, no. 12, pp. 16232–16237, Jun. 2015.
- [1.21] Y.-C. Chi *et al.*, "450-nm GaN laser diode enables high-speed visible light communication with 9-Gbps QAM-OFDM," *Opt. Express*, vol. 23, no. 10, pp. 13051–13059, May 2015.
- [1.22] B. Fahs *et al.*, "A 12-m 2.5-Gb/s lighting compatible integrated receiver for OOK visible light communication links," *IEEE Journal of Lightwave Technology*, vol. 34, no. 16, pp. 3768-3775, Jul. 2016.
- [1.23] POS readers with NFC capabilities. [Online] Available: http://www.truemerchant.com/verifone-vx520/.

CHAPTER 2 ADAPTIVE THRESHOLD DECODING ALGORITHMS

Most previous studies have focused on applications of simultaneous illumination and VLC (SI-VLC) [2.1-2.3]. However, there exist many LED-based display applications, including LCD displays with LED backlights, OLED displays, and micro-LED displays, that can be exploited for VLC, with the LEDs acting as transmitters. The first active matrix LED (AMLED) micro-display with an embedded VLC transmitter was reported in [2.4]. The driver system-on-chip (SoC) drives a wide quarter-VGA display with 400×240 pixels of 30×30 µm² blue gallium nitride (GaN) micro-LEDs, simultaneously supporting 4-bit grayscale image display and VLC at a data rate of 1.25 Mb/s [2.4]. However, on the receiver side, the data recovery of VLC signals from a display presents additional design difficulties compared to lighting-based VLC systems. The main challenge is the varying received signal strength caused by changes in the displayed images or videos.

Intensity modulation (IM) and direct detection (DD) are used in VLC for low complexity. In a simultaneous display and VLC (SD-VLC) system, light from each pixel is superposed at the receiver side in terms of wavelength and path loss through uneven spectral responsivity of the photodiode, producing electrical current. Thus, the image under display directly affects the amplitude of the received VLC signal at the receiver side, which further affects VLC data logic retrieval. Moreover, the amplitude of the VLC signal is also affected by the path loss of the free space, and the uneven spectral responsivity of the photodiode. Different images cause different amplitudes, and the normalized dynamic range of amplitudes can be from 2.5% – 100%. Hence conventional Constant Threshold Decision is not able to recover VLC data correctly and results in poor bit error rate (BER) performance.

To overcome this problem, this chapter presents two Adaptive Threshold Decoding (ATD) algorithms which dynamically adjust the decision threshold voltage: Preamble-based ATD, which utilizes the preamble sequence [2.5], and Section-based ATD, which utilizes the characteristics of OOK modulation and Manchester encoding. The algorithms are verified experimentally using an in-house-developed AMLED micro-LED display VLC transmitter [2.4, 2.5] and a standard photodetector-based VLC receiver. The measured BER of data received from a 4-frame/s micro-LED display is improved from 6.9×10⁻² to 4.4×10⁻⁴ using the Preamble-based ATD algorithm compared to the conventional Constant Threshold Decision scheme, which is further improved to 3.6×10⁻⁴ by using Section-based ATD.

2.1 Simultaneous Display and VLC Overview

2.1.1 Simultaneous Illumination and VLC (SI-VLC) and Simultaneous Display and VLC (SD-VLC) Systems

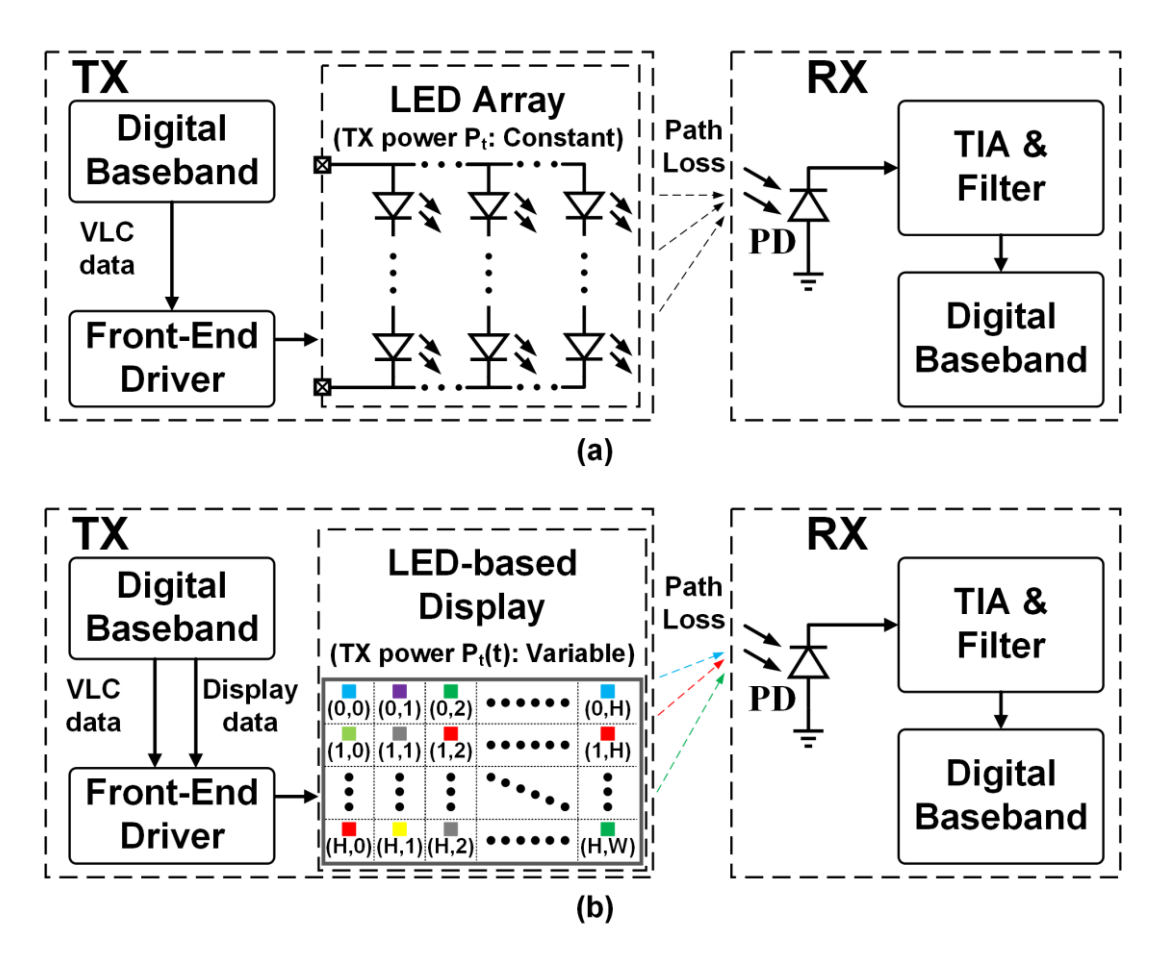


Figure 2.1 (a) A generic simultaneous illumination and VLC (SI-VLC) system, (b) a generic simultaneous display and VLC (SD-VLC) system.

Figure 2.1 shows a generic simultaneous illumination and VLC (SI-VLC) transceiver system and a generic simultaneous display and VLC (SD-VLC) transceiver system. The SI-VLC system is composed of a transmitter (TX) and a photodetector-based receiver (RX), as shown in Figure 2.1(a). The TX consists of a digital baseband for data encoding and signal modulation, and an analog front-end driver to drive the LED array, in which multiple LEDs are connected in series or in parallel to generate sufficient luminous intensity for both illumination and VLC. At the receiver side, the VLC signal with path loss or channel loss is received by a photodetector (PD) and converted into electrical current, which is then converted to voltage and amplified by a trans-impedance amplifier (TIA). After that, a digital baseband is used for data decoding.

In contrast to the SI-VLC system, in the SD-VLC system, as shown in Figure 2.1(b), at the transmitter side, not only VLC data but also display data are fed into the analog front-end driver from the digital baseband. Furthermore, the LED-based display, controlled by the front-end driver, displays still images or videos, and meanwhile, transmits the encoded VLC data. At the receiver side, the VLC signal is received by the receiver (RX), which is the same as that in the SI-VLC system. What's more, due to the same free space optical wireless channel being used in both the SI-VLC and SD-VLC systems, the path loss model is also the same in both systems.

2.1.2 Transmitted Optical Power Difference in SI-VLC and SD-VLC systems

The transmitted optical power is different in SI-VLC and SD-VLC systems. In the SI-VLC system shown in Figure 2.1(a), the transmitted optical power P_t from the LED array is constant, mainly due to the illumination requirements, while in the SD-VLC system in Figure 2.1(b), the transmitted optical power is highly dependent on the displayed content. The LED-based display used in the SD-VLC system can be monochrome or color. Without loss of generality, an LED-based color display consisting of H×W pixels, each individually controllable, is employed as an example. Each pixel, whether consisting of RGB or RGGB sub-pixels, is able to support a large range of brightness and the color gamut, including blue, red, white etc. Hence, for a certain Pixel(i, j), the transmitted optical power spectral distribution or spectral response is variable, dependent on the optical power ratio contributed by the red, green and blue sub-pixels, which are controlled by the display data. And the display data can be considered as a function of time. Thus, $S_{t_{i,j}}(\lambda,t)$ is denoted as the spectral response function over the wavelength of visible light λ for Pixel(i, j), which is also time-varying.

The output current of the PD contributed by the light from Pixel(i, j) is expressed in Eq. (2.1),

$$I_{PD_{i,j},SD-VLC}(t) = PL_{i,j} \int_{\lambda_I}^{\lambda_H} S_{t_{i,j}}(\lambda, t) R_{PD}(\lambda) d\lambda, \qquad (2.1)$$

where $PL_{i,j}$ is the path loss of the optical path from Pixel(i, j) to the PD, which is wavelength-independent and can be considered as a constant value if the locations of Pixel(i, j) and the PD are fixed. Furthermore, due to the uneven responsivity $R_{PD}(\lambda)$ of the PD, the integration accounts for the spectral power distribution of Pixel(i, j), in which λ_L and λ_H are the minimum and the maximum wavelengths of the visible light, respectively.

Consequently, by using superposition, the total output current from the PD at the RX side is estimated in Eq. (2.2),

$$I_{PD,SD-VLC}(t) = \sum_{i=1}^{W} \sum_{i=1}^{H} \left(PL_{i,j} \int_{\lambda_L}^{\lambda_H} S_{t_{i,j}}(\lambda, t) \, R_{PD}(\lambda) \, d\lambda \right). \tag{2.2}$$

The current of the PD $I_{PD,SD-VLC}(t)$ is proportional to the amplitude of the received VLC signal, which means that this amplitude is time-dependent.

For an SI-VLC system, identical LEDs are usually used in the LED array, which means they have the same spectral response. Moreover, the spectral response of illumination LEDs is time-invariant, denoted as $S_t(\lambda)$. Assuming a total of N identical LEDs, then

$$S_{t_1}(\lambda, t) = S_{t_2}(\lambda, t) = \dots = S_{t_N}(\lambda, t) = S_t(\lambda). \tag{2.3}$$

The total output current from the PD at the RX side can be derived by a similar superposition, as shown in Eq. (2.4),

$$I_{PD,SI-VLC} = \sum_{i=1}^{N} \left(PL_i \int_{\lambda_L}^{\lambda_H} S_{t_i}(\lambda) R_{PD}(\lambda) d\lambda \right)$$

$$= \sum_{i=1}^{N} \left(PL_i \int_{\lambda_L}^{\lambda_H} S_t(\lambda) R_{PD}(\lambda) d\lambda \right),$$
(2.4)

where PL_i is the path loss of the optical path from LED(i) to the PD. All LEDs have the same spectral response $S_t(\lambda)$. In contrast to the SD-VLC system, in an SI-VLC system, the amplitude of the received VLC signal, which is in proportion to $I_{PD,SI-VLC}$, is time-independent.

Mathematically, from Eq. (2.2) and Eq. (2.4), the main difference between SI-VLC and SD-VLC systems is whether the amplitude of the received VLC signal is or is not a function of time. Apparently, the conventional Constant Threshold Detection algorithm is not able to recover the VLC data correctly and results in poor BER performance if used in SD-VLC.

2.2 Challenges in Data Recovery from Simultaneous Display and VLC systems

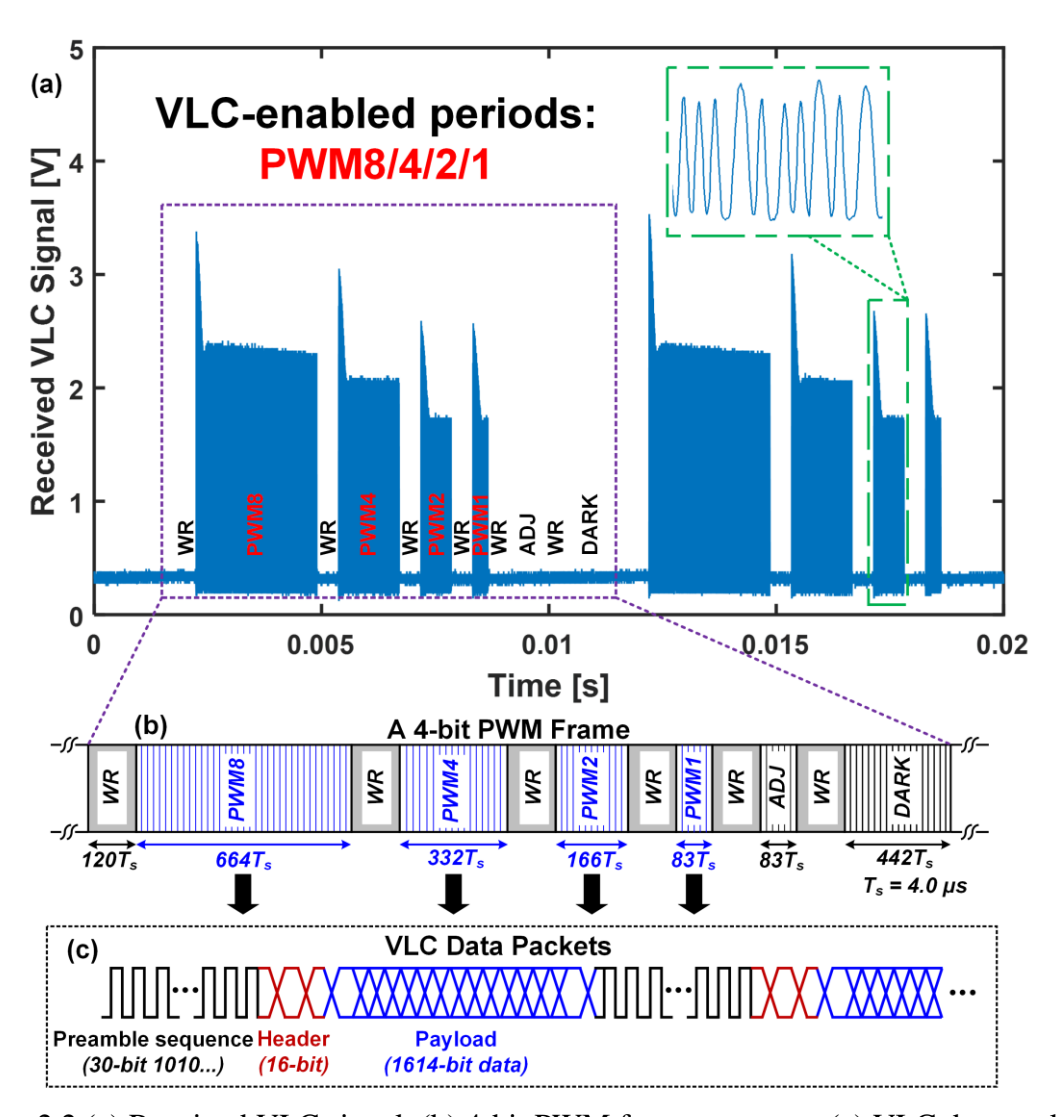


Figure 2.2 (a) Received VLC signal, (b) 4-bit PWM frame structure, (c) VLC data packets.

An in-house-developed AMLED micro-LED display simultaneously supporting VLC function [2.4] is used as a transmitter. The VLC signal is received by a standard photodetector-based receiver, and a corresponding waveform is shown in Figure 2.2(a). To achieve simultaneous display and VLC, a 4-bit pulse-width modulation (PWM) frame structure and VLC data packet format are employed in the AMLED [2.4].

Figure 2.2(b) illustrates the structure of the 4-bit PWM frame, including four binary-weighted display sub-frames PWM8/4/2/1, WRs, adjustable sub-frame (ADJ) and dark sub-frame (DARK). During displayed sub-frames PWM8/4/2/1, which are also VLC-enabled periods, simultaneous VLC is enabled with OOK modulation and Manchester encoding to maintain 50% average brightness, and thus the received VLC signal has a relatively large amplitude in Figure 2.2(a). Therefore, VLC-enabled periods rather than sub-frames PWM8/4/2/1 are used in the remainder of this paper.

WR is the time required to write the display data into the AMLED driver. ADJ and DARK, during which all pixels are turned off, are employed to improve the contrast ratio of the display. Hence, WR, ADJ and DARK are VLC-disabled periods. Consequently, the received signal in these VLC-disabled periods can be considered as 'noise'. Recognizing the VLC-enabled and VLC-disabled periods is one of the most important steps in the proposed algorithms, which are illustrated in detail in the following section. As shown in Figure 2.2(c), in each VLC-enabled period, a data packet format that consists of a 30-bit preamble sequence (1010...), a 16-bit header, and 1614-bit payload VLC data is used to achieve reliable VLC data transmission.

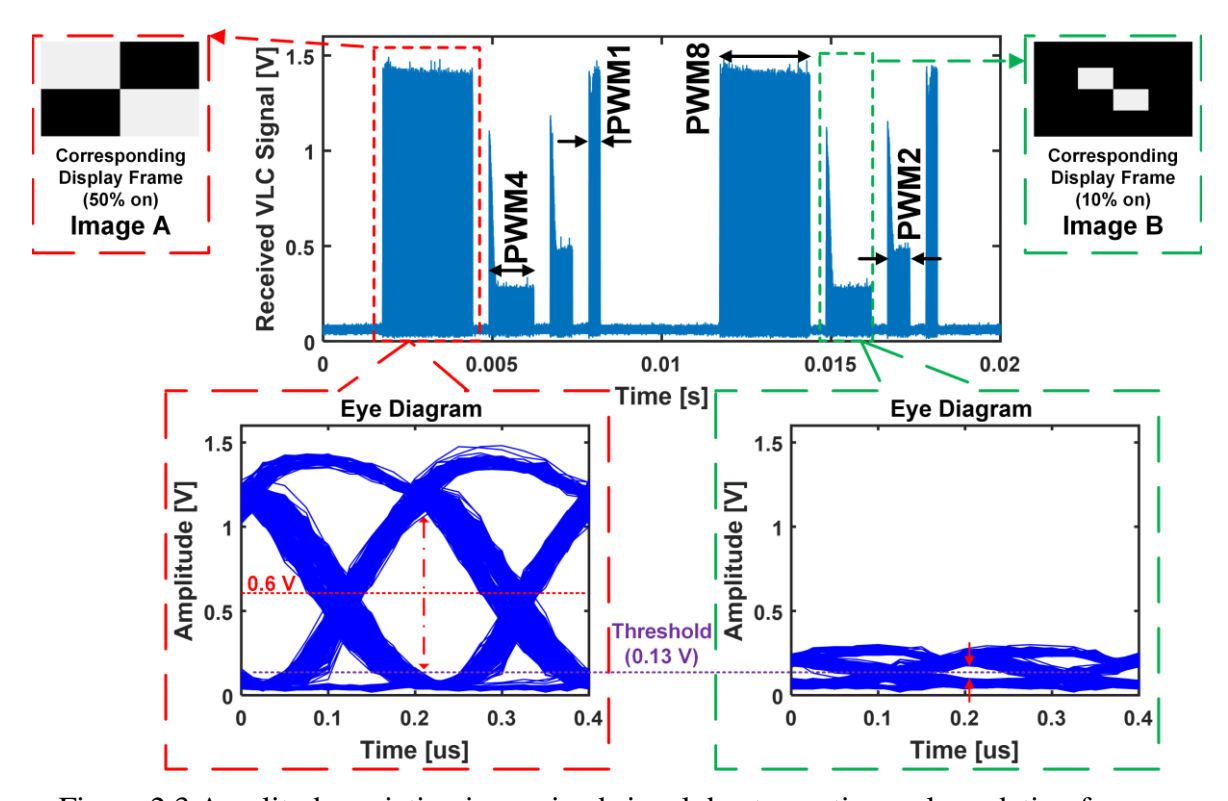


Figure 2.3 Amplitude variation in received signal due to continuously updating frames.

Figure 2.3 shows the amplitude variation of the received VLC signal due to different corresponding displayed frames. Two images, A and B, with 50% and 10% of pixels turned on, respectively, are evaluated as an example. Image A is displayed in VLC-enabled period PWM8, and the corresponding received VLC data Eye Diagram A is shown on the left side, while Image B is displayed in VLC-enabled period PWM4, with the corresponding Eye Diagram B on the right side.

From Eye Diagram A and B, during each VLC-enabled period, the amplitude value of the received VLC signal is relatively constant. Furthermore, both eye diagrams have large eye openings, which means a good signal-to-noise ratio (SNR). However, the amplitude and threshold of the signal in Eye Diagram A is much larger than that in Eye Diagram B. In the former, the optimal threshold value is around 0.6 V, while for the latter, 0.13 V is preferred as the threshold value. If the conventional Constant Threshold Decision algorithm uses the largest threshold from Eye Diagram A, which is around 0.6 V, then all the symbols in PWM4 will be considered as digital '0's. In other words, the data packets in PWM4 will all be rejected, leading to packet loss.

To avoid packet loss and to recover as much VLC data as possible, the conventional Constant Threshold Decision scheme could use the smallest threshold from Eye Diagram B, which is 0.13 V, as shown in Figure 2.3. However, this threshold value cannot recover the VLC data logic of Eye Diagram A correctly. Hence, the conventional Constant Threshold Decision scheme cannot handle amplitude variation.

If a variable or adaptive decision threshold is used for each data period, a higher number of symbols can be recovered correctly, and the BER can be significantly improved. For example in Figure 2.3, the data from Eye Diagram A can be recovered with a threshold close to 0.6 V, whereas a lower threshold of 0.13 V is optimal for Eye Diagram B.

2.3 Proposed Adaptive Threshold Decision Algorithms

To address the limitations of the conventional algorithm, two ATD algorithms, Preamble-based and Section-based, are proposed, both recognizing the VLC-enabled periods by using the trigger level, while calculating the proper threshold values using different schemes.

2.3.1 Preamble-based ATD Algorithm

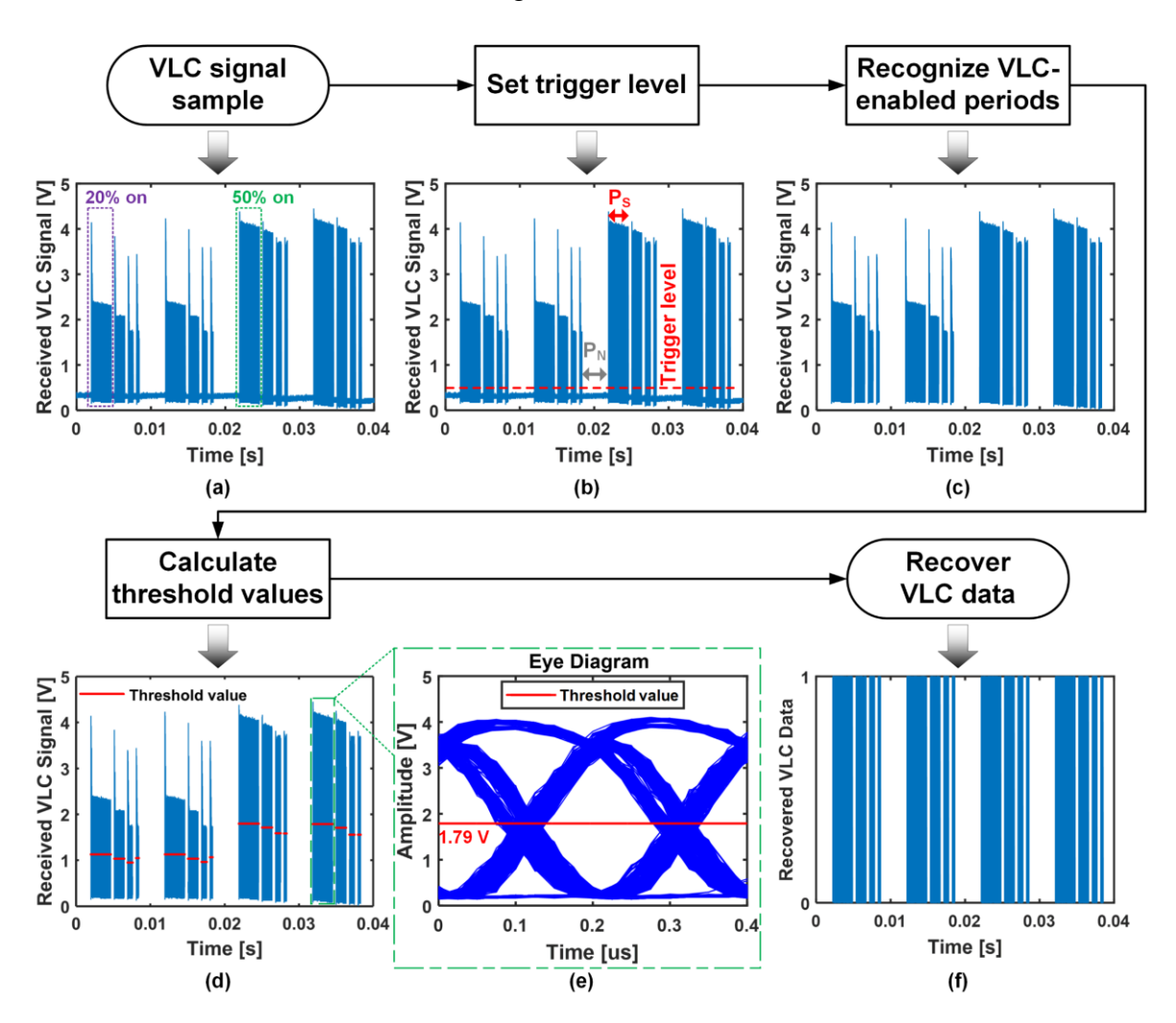


Figure 2.4 Flow chart of the proposed Preamble-based Adaptive Threshold Decision algorithm, (a) received signal sample, (b) set trigger level for recognition, (c) recognized VLC-enabled periods, (d) calculated threshold values from Preamble-based ATD, (e) eye diagram with a calculated threshold voltage of 1.79 V, (f) recovered VLC data.

The Preamble-based ATD algorithm dynamically adjusts the decision threshold voltage by utilizing the preamble sequence, as shown in Figure 2.4. VLC signal data from the experiment is used as an example to illustrate the algorithm.

First, the original VLC signal data is sampled from the RX front-end, and the corresponding waveform of the sample is shown in Figure 2.4(a). Then, a trigger level above the noise level is obtained to help recognize VLC-enabled periods. For the VLC-disabled periods or noise periods (P_N) in Figure 2.4(b), all the sample points are below the trigger level, while for the VLC-enabled periods (P_S) in Figure 2.4(b), signal amplitudes are higher than the trigger level, as are some sample points of logic '1'.

Based on these characteristics, boundaries between neighboring P_S and P_N, which define the start and end of all P_S, can be found. VLC-disabled periods are considered as 'noise' and rejected, and VLC-enabled periods are recognized, as shown in Figure 2.4(c).

Next, proper threshold values are calculated by averaging the 30-bit preamble (1010...) at the beginning of each VLC-enabled period. These calculated threshold values with the corresponding VLC signal are shown in Figure 2.4(d), ranging from 0.96 V to 1.79 V. In each period, the threshold value is approximately 50% of the corresponding amplitude. Hence the VLC data can be recovered much better. For example, the calculated threshold voltage of 1.79 V is close to the optimal threshold of the eye diagram, as referred to in Figure 2.4(e). Finally, the VLC logic data is retrieved, as shown in Figure 2.4(f), and the BER is computed.

The key parts of the Preamble-based and Section-based ATD algorithms are recognizing the VLC-enabled periods by using the trigger level, and calculating the proper threshold values based on the recognized data periods. Conventional Automatic Gain Control (AGC) is widely used in wireless communication systems. However, AGC cannot tell the difference between VLC-enabled and VLC-disabled periods, and it will amplify both of them. Besides, due to the variation of amplitude and threshold, the VLC data cannot be recovered correctly on the receiver side by using constant threshold decoding algorithm.

The Preamble-based ATD algorithm calculates the threshold values by averaging the preamble sequences. Thus one VLC-enabled period only has one threshold value. However, if the amplitude of the received VLC signal changes in one data period, which is mainly due to the changes of the distance or the angle between the TX and RX, then the Preamble-based ATD algorithm cannot handle it.

2.3.2 Section-based ATD Algorithm

Due to the OOK modulation and Manchester encoding used in AMLED system to maintain 50% average brightness at any small period, a scheme to calculate threshold values in each VLC-enabled period is to divide the period into several sections or sub-periods first and then average the signal (no matter whether it is a preamble, header or payload data) in every section, which is called the Section-based ATD algorithm. The number of VLC symbols in each section should be moderate; too large a number may not follow the change of amplitude, while too small a number may not guarantee the equal probabilities of logic '1' and '0' in each section and will consume more computation.

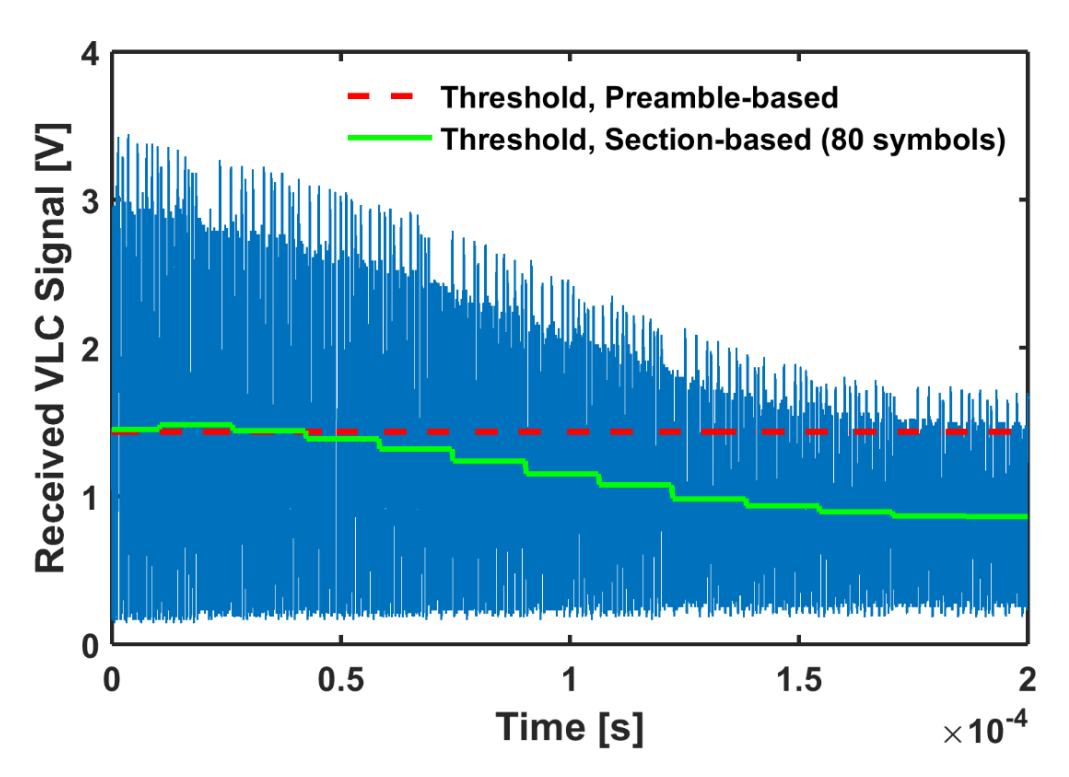


Figure 2.5 Received VLC signal with thresholds from Preamble-based and Section-based ATD algorithms.

Figure 2.5 shows the threshold comparison of the Preamble-based ATD and Section-based ATD algorithms with amplitude variation in one VLC-enabled period. In this VLC-enabled period, the amplitude decreases with time. A threshold value computed from the Preamble-based ATD algorithm is shown in Figure 2.5 by the red dashed line. For those signals after $t=1.5\times10^{-4}$ s, the algorithm is not able to recover the logic correctly because the constant threshold value is close to the amplitude of the received signal.

The threshold values, calculated using the Section-based ATD scheme, each section with 80 symbols, drop step by step, following the decreasing signal amplitude. These threshold values are always appropriately 50% of the varying amplitude in the range from 0 s to 2×10^{-4} s, which allows recovery of more symbols compared with the threshold using Preamble-based ATD.

2.4 Experiments and Results

2.4.1 Experiment Setup

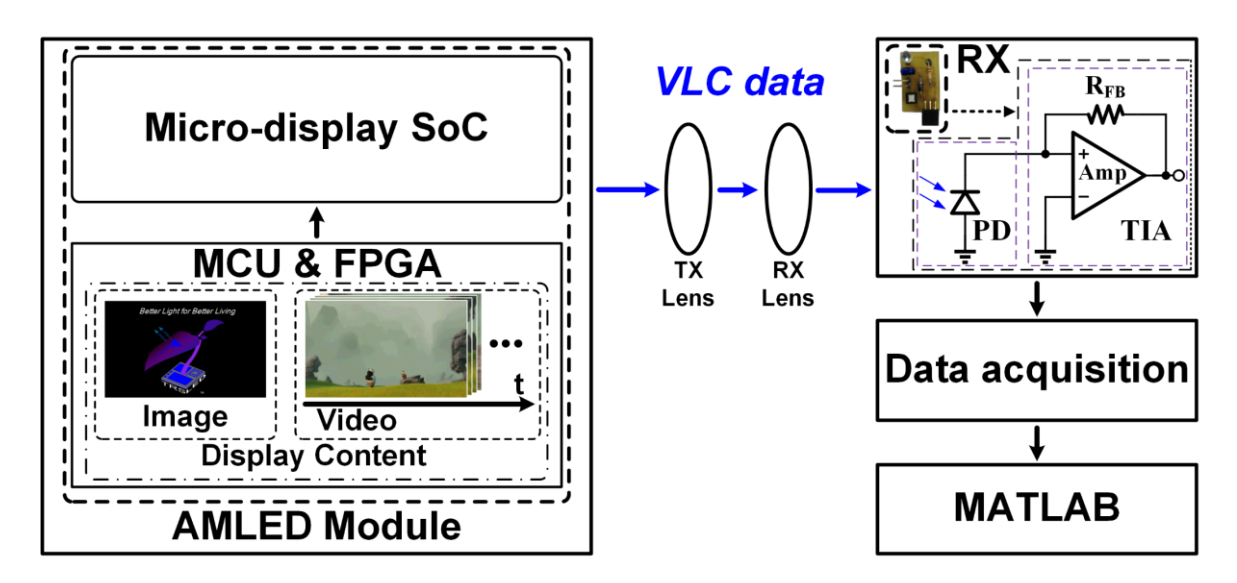


Figure 2.6 Block diagram of simultaneous display and VLC experimental setup.

Figure 2.6 depicts the block diagram of the concurrent VLC and display experimental setup. An AMLED module, consisting of a micro-display SoC, micro-controller unit (MCU) and field-programmable gate array (FPGA), is used as a transmitter, which supporting simultaneous display and VLC [2.4].

The displayed content, whether a still image or video, is programmed into the micro-display SoC through the MCU and FPGA. Each of the micro-LED pixels in the micro-display SoC is controlled individually to display the corresponding content from the MCU and FPGA, and at the same time, transmit the VLC data at 5 Mb/s using OOK modulation and Manchester encoding. Pseudorandom binary sequence 7 (PRBS-7) pattern is used in the measurement.

On the receiver side, the VLC signal through the optical free space channel is received by the receiver (RX) front-end, which consists of a PD and a TIA. Next, data acquisition is performed with a 40 MS/s sample rate for offline decoding using MATLAB. Testing is performed with and without lenses. The AMLED module displays testing image patterns and transmits VLC data. The received VLC data is then decoded using the proposed ATD algorithms, and the BER is evaluated.

2.4.2 Results and Discussion

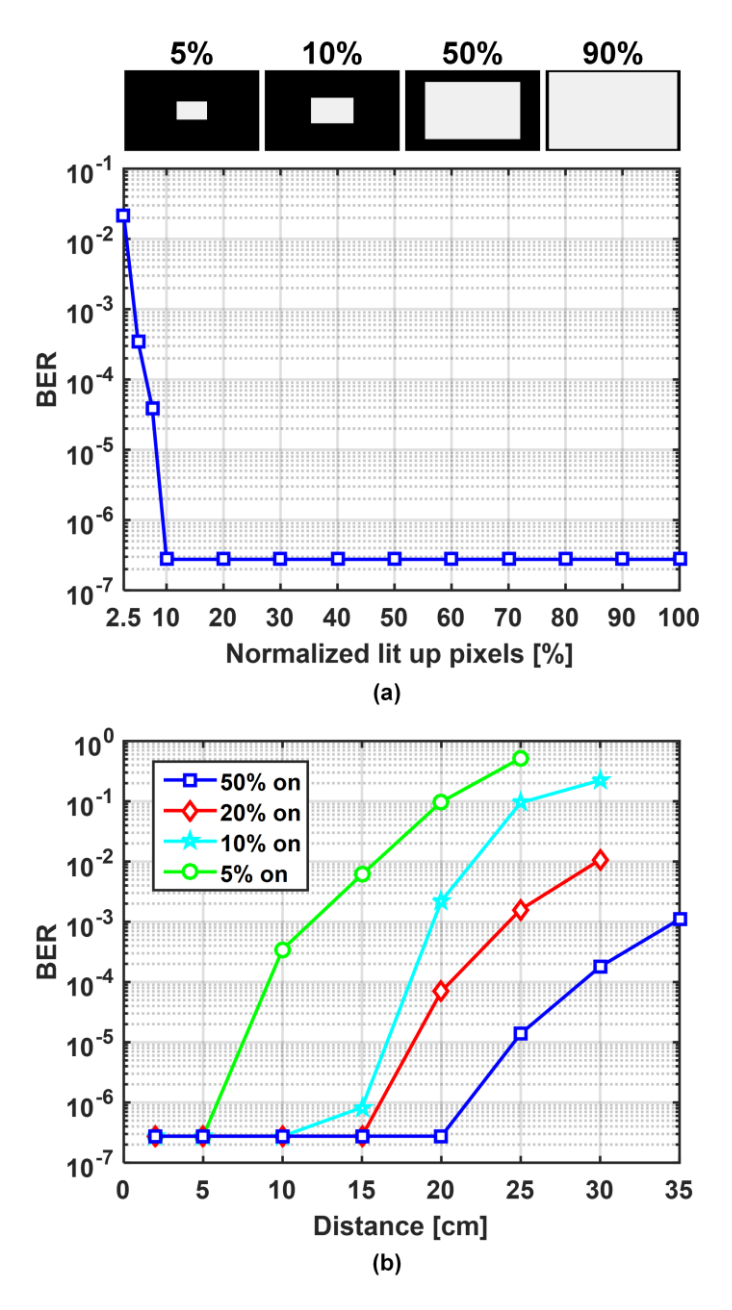


Figure 2.7 (a) BER vs. normalized lit up pixels at 10 cm distance, (b) BER vs. distance.

For all the BER measurement in this chapter, the number of collected bits is around 100 times larger than the reciprocal of the BER, except for the best BER of 2×10^{-7} , which has 25 M collected bits to save the measurement time. For example, if the BER result is 10^{-5} , then collected bit number is around 10 M. As mentioned before, there are VLC-enabled and VLC-disabled periods and the average data rate of gen-1 AMLED VLC transmitter is 1.25 Mb/s. Thus it takes 8 seconds for the gen-1 AMLED to transmit 10 M bits. Furthermore, due to the offline decoding, it takes more time for data acquisition and decoding using proposed ATD algorithms.

When the displayed content is a still image, received VLC data is decoded using the proposed Preamble-based ATD algorithm. Figure 2.7(a) depicts the BER results for still images with different percentages of lit up pixels ranging from 2.5% to 100%, at a 10 cm distance. When the percentage of normalized lit up pixels is larger than 10%, the BER can be 2×10^{-7} . And the data acquisition is stopped once get 25 M bits to save the required time for measurement. Thus, the measured BER results of still images with lit up percentage larger than 10% are the same as 2×10^{-7} , as shown in Figure 2.7(a). Actually, the BER should decrease as the lit up pixels increase, which can be observed if more bits are collected.

Figure 2.7(b) shows the BER results for four still images with different percentages of lit up pixels at distances ranging from 2 cm to 35 cm. To achieve a BER $< 10^{-4}$ without lenses, the distance is up to 20 cm for the image with 20% of pixels on and around 25 cm for the image with 50% of pixels on. To save the measurement time, the maximum number of collected bits for BER calculation is 25 M, that's why the best BER is 2×10^{-7} in Figure 2.7(b). And if more bits are collected, better BER can be observed in the measurement.

Table 2.1 VLC BER Comparison for AMLED Micro-Display System with 4-frame/s.

	Lenses	Range	Conventional Constant Threshold	Preamble-based Adaptive Threshold	Section-based Adaptive Threshold
DED	w/o	2 cm	6.9×10 ⁻²	4.4×10 ⁻⁴	3.6×10 ⁻⁴
BER	W	40 cm	8.2×10 ⁻²	1.8×10 ⁻³	1.7×10 ⁻³

When the displayed content is a 4-frame/s video, the frames have variable lit up pixel percentages. Hence amplitude variation happens in the received signal, as mentioned before. The same received VLC data is decoded by the conventional Constant Threshold Decision, proposed Preamble-based ATD and Section-based ATD algorithms. The number of received bits is around 25 M, which takes 20 seconds for transmission in gen-1 AMLED micro-display system.

Table 2.1 gives the BER results comparison of the algorithms. In the cases of 2 cm without lenses and 40 cm with lenses, the BER is significantly improved by using the ATD algorithms compared with the conventional Constant Threshold scheme.

Compared with the Constant Threshold scheme, in the case of 2 cm without lenses, the Preamble-based ATD algorithm improves the BER performance from 6.9×10^{-2} to 4.4×10^{-4} , which is further improved to 3.6×10^{-4} by using the Section-based ATD. While in the case of 40 cm with lenses, for the same VLC signal samples, the BER performance is evaluated as 8.2×10^{-2} , 1.8×10^{-3} and 1.7×10^{-3} using the conventional Constant Threshold Decision, Preamble-based ATD and Section-based ATD, respectively.

In Figure 2.7(b), BER of 2.8×10^{-7} is achieved for the still images with 5% of pixels on at 2 cm distance, by using Preamble-based ATD algorithm, while for the BER results of a 4-frame/s video in Table 2.1, BER performance is calculated as 4.4×10^{-4} at the same distance of 2 cm by using Preamble-based ATD algorithm. One of the reasons for the large BER difference shown in Table 2.2 is that the 4-frame/s video actually consists of many still image frames with different percentages of lit up pixels, and some of them may with low percentages, which means small optical power. Furthermore, the frame rate may also affect the BER performance, still images are 0-frame/s, while the video used in Table 2.1 is 4-frame/s.

Table 2.2 BER Difference for Still Image and 4-frame/s Video

	Lenses	Range	Still image with 5% on	4-frame/s video
BER	w/o	2 cm	2.8×10 ⁻⁷	4.4×10 ⁻⁴

As mentioned above, the traditional Constant Threshold Decision algorithm cannot handle variable amplitudes, which either leads to data packet loss or poor BER performance. The proposed Preamble-based ATD algorithm is able to recognize the VLC-enabled periods and calculate the threshold values by averaging the preamble sequence at the beginning of each data period. Thus, a certain 'constant' threshold value is actually applied in the corresponding VLC-enabled period, which only works under the assumption that the amplitude variation is quite small in each data period. The proposed Section-based ATD algorithm, on the other hand, recognizes the VLC-enabled period with the same method as the Preamble-based ATD, and averages the signal in each section to produce the corresponding threshold values. However, the Section-based ATD algorithm requires larger computation and power.

References

- [2.1] A. M. Khalid, G. Cossu, *et al.*, "1-Gb/s transmission over a phosphorescent white LED by using rate-adaptive discrete multitone modulation," *IEEE Photonics Journal*, vol. 4, no. 5, pp. 1465–1473, Oct. 2012.
- [2.2] J. Grubor, S. C. J. Lee, K.-D. Langer, *et al.*, "Wireless high-speed data transmission with phosphorescent white light LEDs," in *European Conference on Optical Communication*, Sept. 2007, pp.1–2.
- [2.3] H. L. Minh, D. O'Brien, *et al.*, "100-Mb/s NRZ visible light communications using a postequalized white LED," *IEEE Photonics Technology Letters*, vol. 21, no. 17, pp. 1063–1065, Aug. 2009.
- [2.4] X. Li, L. Wu, Z. Liu, B. Hussain, W. C. Chong, K. M. Lau, and C. P. Yue. "Design and characterization of active matrix led microdisplays with embedded visible light communication transmitter." *Journal of Lightwave Technology*, vol. 34, no. 14, pp. 3449–3457, 2016.
- [2.5] L. Sun, X. Li, B. Hussain, and C. P. Yue, "An adaptive threshold decoding algorithm for visible light communication data recovery from LED-based display systems," accepted for presentation at *IEEE Photonics Conference (IPC)*, Oct., 2017.

CHAPTER 3 MICRO-DISPLAY SYSTEM WITH VISIBLE LIGHT COMMUNICATION CAPABILITY

There exist many LED-based display applications, including LCD displays with LED backlights, OLED displays, and micro-LED displays, that can be exploited for the deployment of VLC, with the LEDs acting as transmitters. Due to the exponential growth in demand for wearable devices and virtually reality (VR) applications, active matrix light-emitting diode (AMLED) micro-display using micro-LEDs has recently attracted a great deal of research interest. Micro-LED based micro-displays have unique advantages compared with liquid crystal displays (LCDs). First, the diameter of a micro-LED is usually only tens of micrometers; hence it is possible to implement display panels with high pixels per inch (PPI) by fabricating a large-size micro-LED array on a single substrate. Second, unlike LCDs using LEDs as backlights, micro-LED based micro-displays are self-emissive, displaying bright images without an external light source, and are thus thinner and smaller [3.1]. Moreover, compared with illumination LEDs, micro-LEDs have a relatively large modulation bandwidth, and can be used as transmitters for VLC.

The first AMLED micro-display with an embedded VLC transmitter was reported in [3.2], with a 5 Mb/s modulation bit rate. This chapter presents a second-generation AMLED micro-display system, consisting of a proposed CMOS AMLED driver integrated with an on-chip power management unit (PMU), and a flip-chip bonded blue gallium nitride (GaN) micro-LED array with 36×64 pixels each measuring of 40×40 µm², for simultaneous display and VLC applications. The AMLED driver consists of a row driver, column driver and pixel drivers with 36×64 pixels. Measurement results show that the proposed pixel driver with bandwidth expansion techniques can achieve a 20 Mb/s bit rate at 10 cm, which is four times as large as the 5 Mb/s modulation bit rate in [3.2].

3.1 AMLED Micro-display System Overview

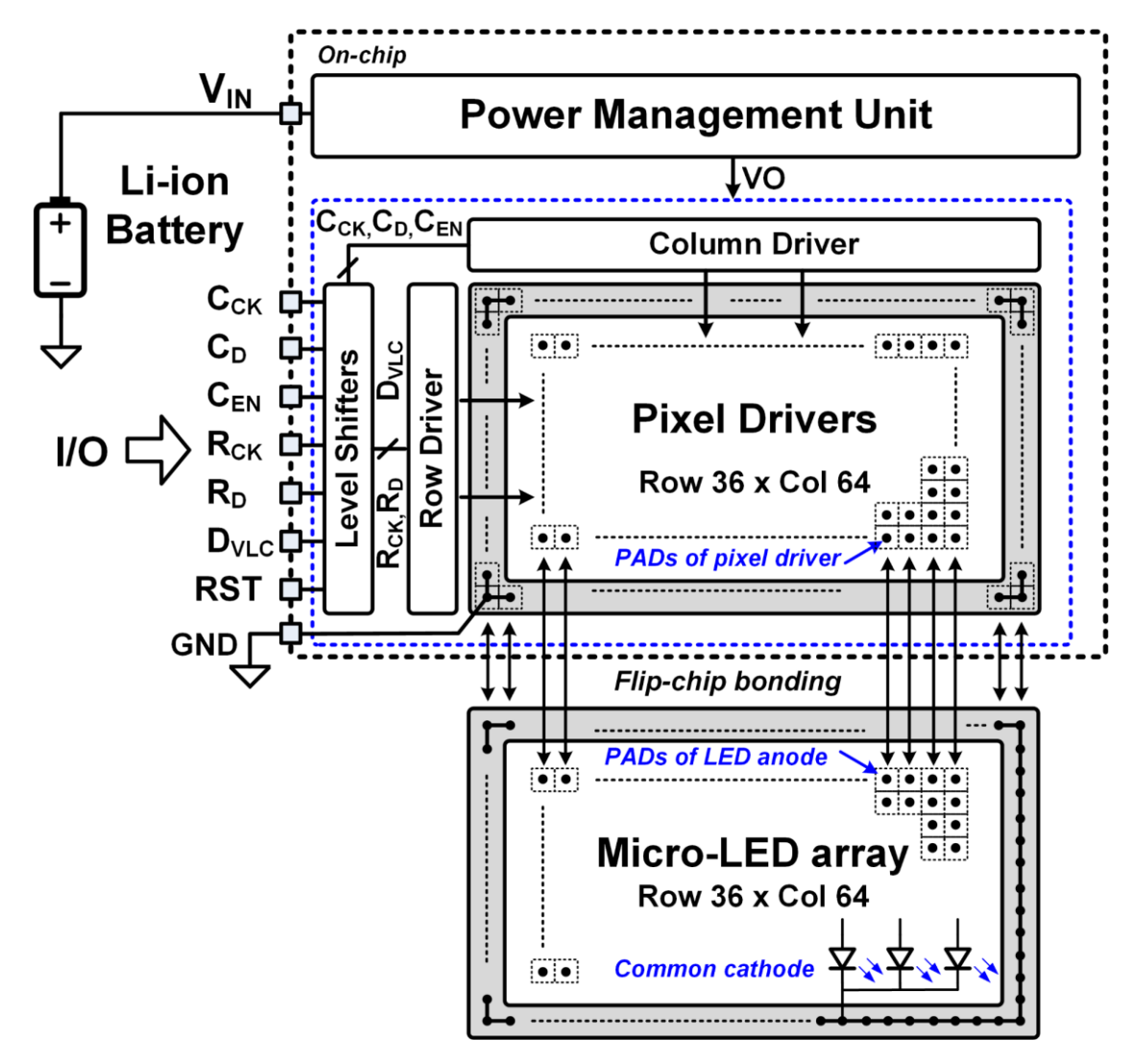


Figure 3.1 System architecture of proposed AMLED micro-display system.

Figure 3.1 shows the architecture of the proposed AMLED micro-display system composed of a CMOS system-on-chip (SoC), and a micro-LED array. The figure shows the SoC consisting of an on-chip power management unit (PMU) and an AMLED driver, with a row driver, a column driver, and 36×64 pixel drivers. Each pixel driver has a pad on the top with the opening exposed to the air, for flip-chip bonding. The SoC is implemented in a 0.18-μm CMOS process.

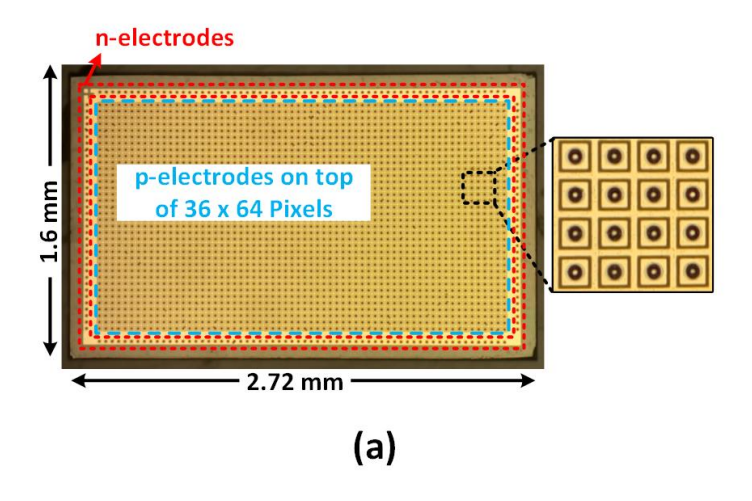
In the micro-LED array, with 36×64 pixels on the center area built on a GaN substrate, each micro-LED has its own anode and shares a common cathode which is arranged to the circumference. Each micro-LED is flip-bonded on the same location as the pixel driver. The pixel drivers are powered by the PMU built on the same silicon that provides a stable internal voltage VO [3.1].

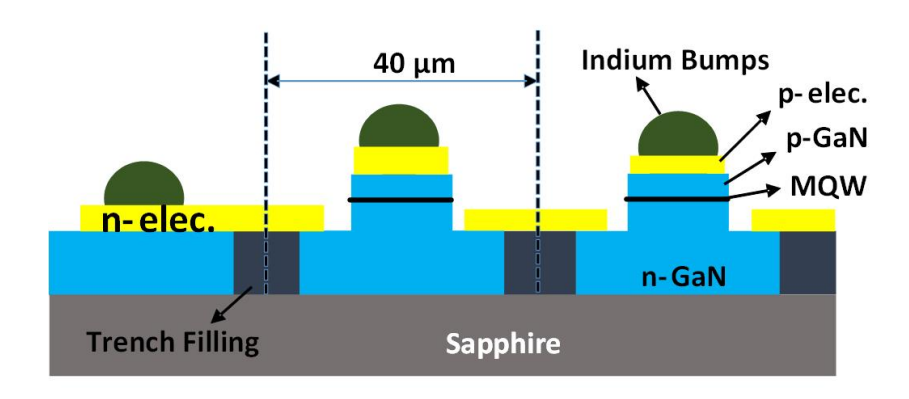
The display data and VLC data are fed into the AMLED micro-display system through the I/O pins (C_{CK}, C_D, C_{EN}, R_{CK}, R_D, D_{VLC}, and RST). Row and column drivers are used to write the display data to all the pixels by row-by-row progressive scanning. For compatibility with the output voltage level of the off-chip controller, high to low level shifters are used to convert the input signal to the internal voltage level. The PMU provides an internal voltage VO from the Li-ion battery voltage ranging from 2.7V to 4.2V [3.1, 3.3].

3.2 Features of Micro-LEDs

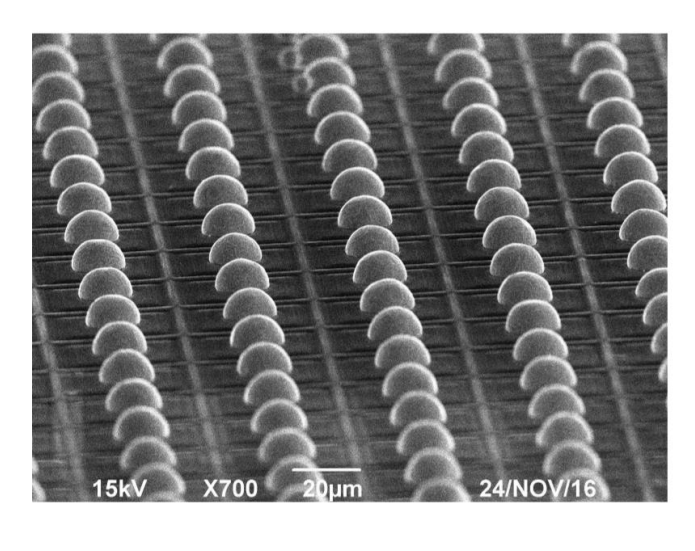
Figure 3.2(a) shows the micrograph of the micro-LED array consisting of 36×64 pixels, each measuring 40μm×40μm. All the micro-LED pixels are uniformly distributed in the central area with p-type electrodes covering the top, while n-type electrodes are connected to the circumference of the micro-LED array. Figure 3.2(b) shows the cross-sectional diagram of the micro-LED array with indium bumps. The micro-LED array adopts a common-cathode design. All the p-type electrodes of the micro-LED pixels are covered with indium bumps for the flip-chip bonding process, as are the n-type electrodes located at the circumference of the micro-LED array. Pixels, fabricated by n-GaN on a sapphire substrate, are isolated by ICP etching down to the sapphire, and each trench is filled by a black mixture of three kinds of color filter (red, green, blue), which can suppress the crosstalk between pixels [3.1]. Moreover, to further reduce the crosstalk, the sapphire substrate is thinned down to around 150 μm before being flip-chip bonded to the AMLED driver. And the Cr/Al-based p-type electrodes are used to provide high reflectivity to increase light extraction efficiency.

For the flip-chip bonding process, an Au-In metal bonding scheme is adopted. After the indium deposition on the p-electrode of each pixel, the indium bumps are formed though a reflow process in a furnace at 170 °C for one second in a formic acid ambient. The scanning electron microscope (SEM) image of the micro-LED array with indium bumps after the reflow process is shown in Figure 3.2(c). The micro-LED array on the sapphire substrate is then flip-chip bonded onto the silicon IC by using Au-In metal bonding [3.1].





(b)



(c)

Figure 3.2 (a) Micrograph of micro-LED array, (b) cross sectional diagram of the micro-LED array with indium bumps, (c) SEM of micro-LED array with indium bumps after reflow process.

3.2.1 I-V Characteristics of Micro-LEDs

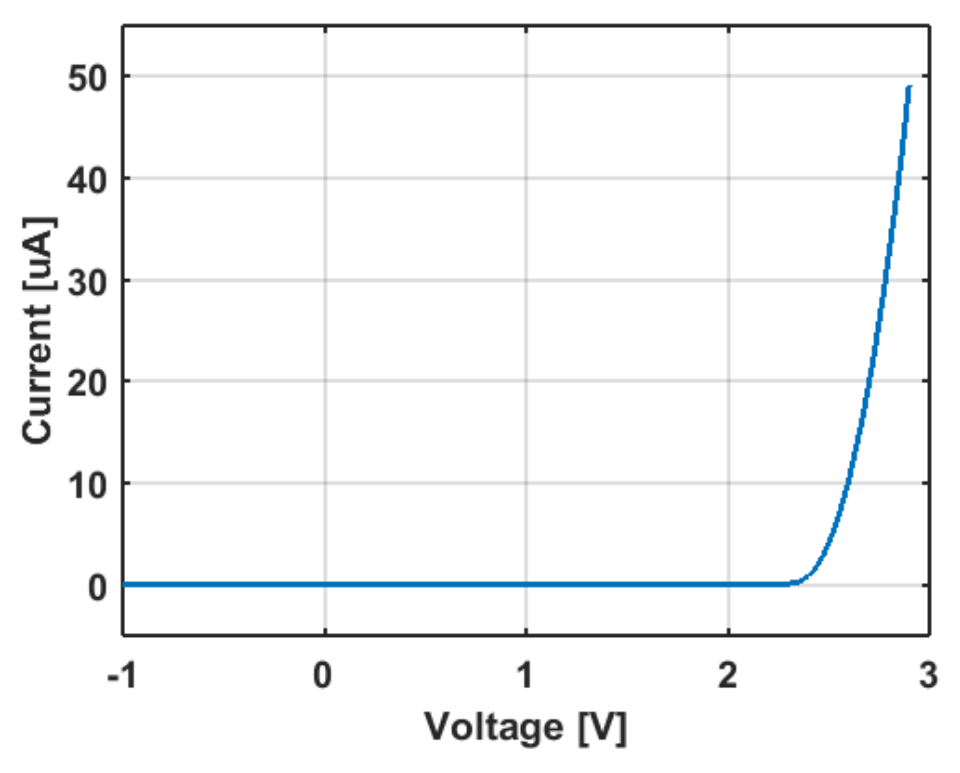


Figure 3.3 Measured I–V characteristics of Micro-LEDs.

The measured I-V curve of a micro-LED pixel is shown in Figure 3.3. The forward voltage of the micro-LED is 2 V with ~400 pA. When the micro-LED is biased at 2.6 V, the current is around 10 μ A, while the micro-LED is biased at 2.7 V with a current of 20 μ A.

For these micro-LEDs used for micro-display applications, a small current cannot provide enough optical power for display, while too large a current may damage human eyes. Thus, the current should be around several tens of microamperes. The turn-on voltage of the micro-LED is appropriately 2.1 V, with a forward current value of 90 nA.

3.2.2 C-V Characteristics of Micro-LEDs

The measurement of the C-V characteristics of micro-LEDs is performed as follows: the micro-LED under testing is biased at a fixed DC voltage first. Then a small amplitude AC voltage is applied across the micro-LED, and the corresponding AC current is measured. Finally, the impedance of the micro-LED is calculated, which is interpreted in terms of a parallel combination of a capacitance and a conductance.

The measured C-V curve of a micro-LED pixel is shown in Figure 3.4. The parasitic capacitance value of the micro-LED changes with the DC bias voltage. It increases with a DC bias voltage ranging from -1 V to 2.1 V. However, for a DC bias voltage larger than 2.1 V, the micro-LED is turned on and the DC current dominates, making the conductance in the impedance significant. The measured capacitance even could be negative, which is called negative capacitance (NC) effect, observed in a variety of semiconductor devices [3.4]. Considering the forward current of the micro-LEDs in display applications, which is several tens of microamperes, and the parasitic capacitance above 2 pF, micro-LEDs are not able to be modulated at a high data rate.

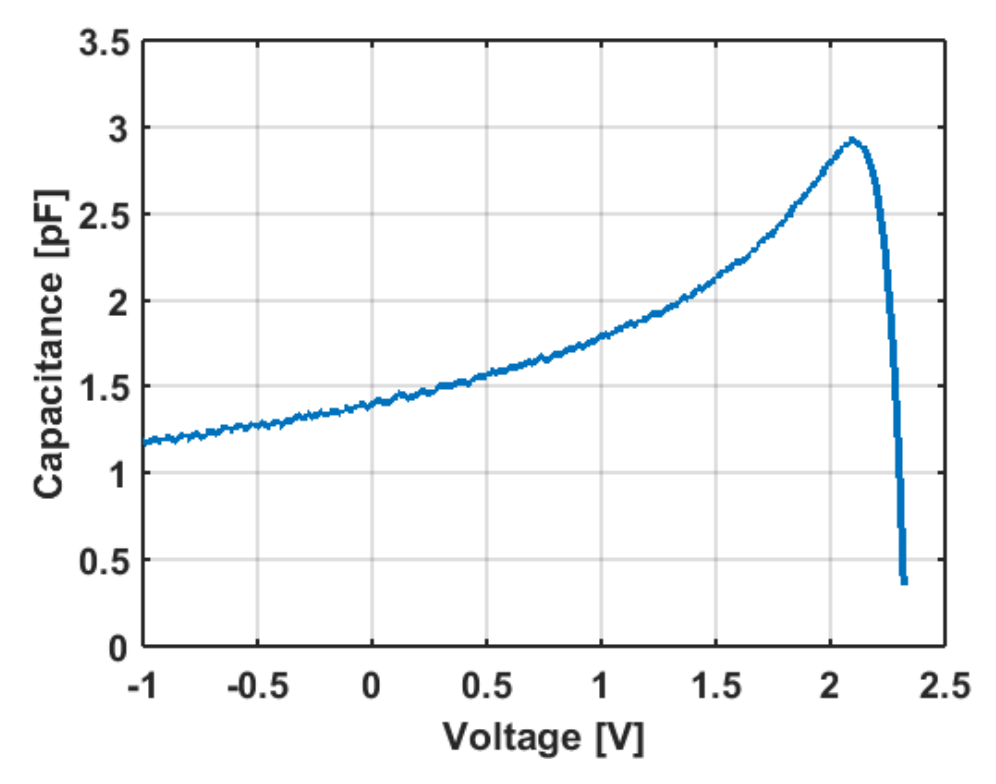


Figure 3.4 Measured C-V characteristics of micro-LEDs.

3.2.3 First Order Equivalent Circuit

As shown in Figure 3.3 and Figure 3.4, micro-LEDs in display application have a forward current value of 5 μ A at 2.5 V forward voltage, with the parasitic capacitance above 2 pF.

The parasitic capacitance of a micro-LED is voltage-dependent, as described by Eq. (3.1),

$$C(V) = \frac{Q}{V},\tag{3.1}$$

where Q denotes the electrical charges on the parasitic capacitor, V is the voltage across the micro-LED, and C(V) is the parasitic capacitance of the micro-LED.

Intensity modulation (IM) and direct detection (DD) are used in VLC for low complexity. The light intensity of micro-LEDs, which is in proportion to the forward current, is modulated in OOK modulation. According to the characteristics of the micro-LED shown in Figure 3.3, the voltage *V* across the micro-LED is not able to maintain a constant value when the forward current is modulated.

Thus, during the charging or discharging process, Eq. (3.2) is derived as

$$\int C(V)dV = \int i(t)dt, \qquad (3.2)$$

where the current charging the parasitic capacitance C(V) is denoted as i(t), which is timevarying.

Considering the first-order effect in the micro-LED, to estimate the charging and discharging time, C(V) can be simplified as a constant value C. Hence, Eq. (3.2) is simplified as Eq. (3.3),

$$\int dV = \frac{\int i(t)dt}{C}.$$
(3.3)

Moreover,

$$\Delta V = \int_{t_s}^{t_e} dV = \frac{\int_{t_s}^{t_e} i(t)dt}{C} \le \frac{i_{max}\Delta t}{C_{min}},$$
(3.4)

where t_s and t_e are the start and end of the charging/discharging period, respectively, ΔV is the difference in voltage across the micro-LED at t_s and t_e , i_{max} is the maximum value of the current from t_s to t_e , and $\Delta t = t_e - t_s$.

For the micro-LEDs in [3.2], $i_{max} = 5 \mu A$, $\Delta V = 0.3 \text{ V}$, and C_{min} is around 2 pF; hence,

$$\Delta t \ge \frac{\Delta V C_{min}}{i_{max}} = \frac{0.3 \times 2p}{5\mu} = 0.12\mu s.$$
 (3.5)

Thus, the corresponding data rate is expressed as Eq. (3.6),

$$f_D = \frac{1}{\Delta t} \le \frac{1}{0.12\mu} = 8.33 Mbit/s$$
 (3.6)

The data rate f_D is smaller than the maximum value of 8.33Mb/s. And the modulation symbol rate of the micro-LEDs in [3.1] is limited at 5 Mb/s.

Eq. (3.4) provides a basic understanding of the bandwidth limitations in the micro-LEDs with low current density. To expand the bandwidth of the micro-LED, it is intuitive to increase the forward current i(t) and limit the voltage change ΔV . These two guidelines are employed in the following pixel driver design.

Figure 3.5 shows the first-order equivalent circuit of the micro-LED, in which a large parasitic capacitance is considered.

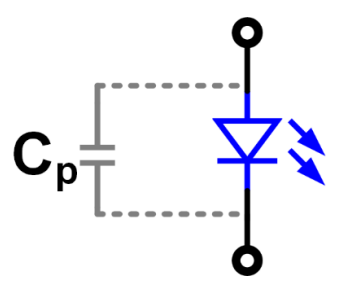


Figure 3.5 First-order equivalent circuit of the micro-LED.

3.3 CMOS AMLED Driver

The CMOS AMLED driver consists of a row driver, a column driver, and 36×64 pixel drivers. The display data is loaded into the pixel drivers through the row and column driver, via row-by-row progressive scanning.

3.3.1 Design and Timing of Row Driver

With the input data R_D and clock signal R_{CK} , the row driver can generate row selection signals to enable the rows one by one. The outputs of the row driver are the row selection signals R_{SEL} . Figure 3.6 shows the diagram of the row driver, which consists of a 36-bit shift register and 36 level shifters. The shift register is composed of 36 D flip-flops and 35 digital buffers. The output of the D flip-flop is buffered by the digital buffer, and then connected to the D flip-flop of the next stage, and so on. The input of the first stage D flip-flop is connected to R_D , which is the data for the row driver. And all the D flip-flops share a common clock signal R_{CK} . Moreover, low to high level shifters are used to convert the outputs of all the D flip-flops to the row selection signals R_{SEL} . $R_{SEL}[0] - [35]$ control the pixel drivers.

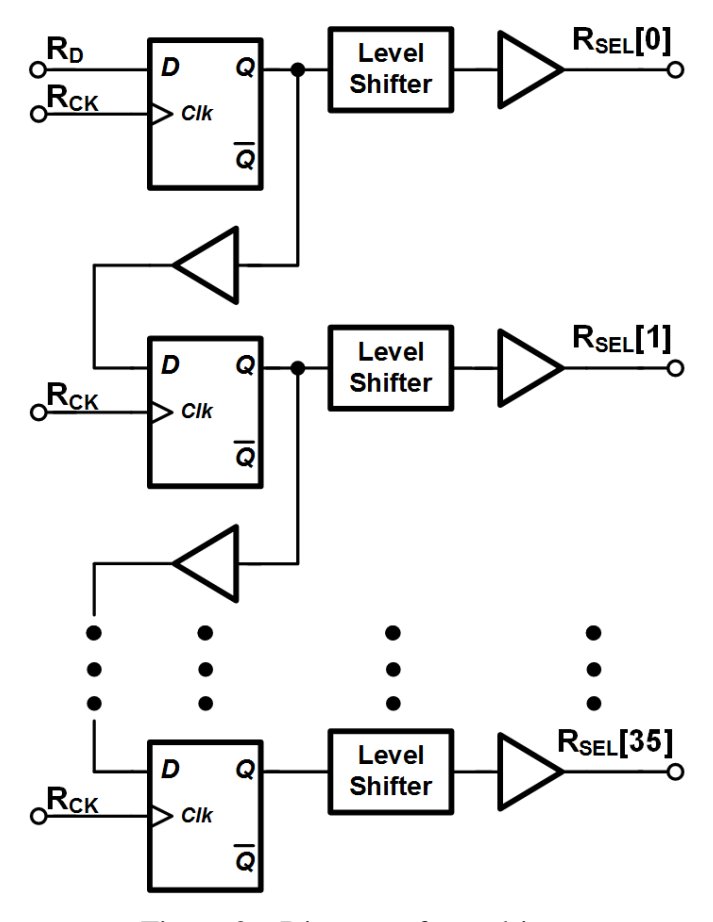


Figure 3.6 Diagram of row driver.

The timing of the row driver is shown in Figure 3.7. Row-by-row progressive scanning is used to write the display data into the AMLED driver. When the value of R_{SEL}[i] is logic '0', it means that *Row i* is enabled, and the display data of the pixels in *Row i* will be loaded into the pixel drivers through the column driver, which is described in detail in the following section. In Figure 3.7, R_{SEL}[0] and R_{SEL}[1] become logic '0' in turn, and this is maintained during one clock period without any overlap. Hence, at most, one row is enabled at any moment, ensuring that display data can be fed into the pixel drivers correctly.

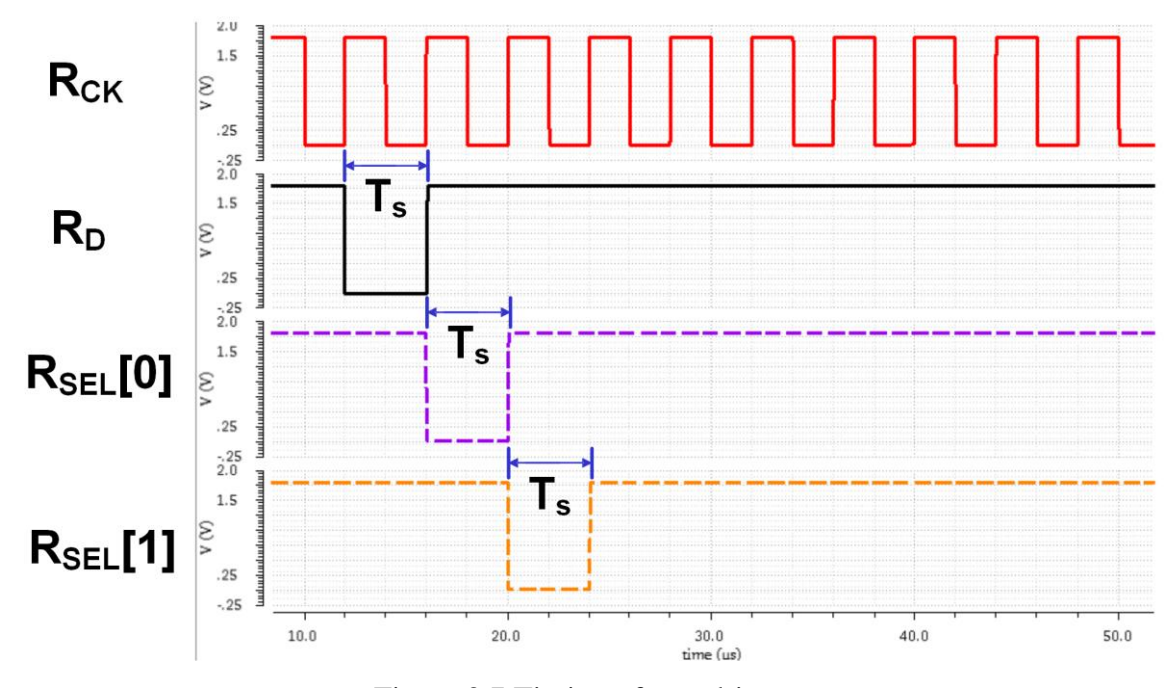


Figure 3.7 Timing of row driver.

3.3.2 Design and Timing of Column Driver

With the clock signal C_{CK} and column enable signal C_{EN} , serial input data C_D is converted and saved as 64-bit display data for the pixels in one row, which is $C_{DATA}[0]$ to $C_{DATA}[63]$. Figure 3.8 shows the diagram of the column driver, which consists of a 64-bit shift register and 64 level shifters. The shift register is composed of 64 D flip-flops and 63 digital buffers. The output of one D flip-flop is buffered by the digital buffer, and then connected to the D flip-flop of the next stage, and so on. The input of the first stage D flip-flop is connected to C_D . When C_{EN} is enabled, the outputs of the 64 D flip-flops are loaded and converted to column display data $C_{DATA}[0] - [63]$ through another 64 D flip-flops and level shifters. And all the D flip-flops share a common clock signal C_{CK} . $C_{DATA}[0] - [63]$ are the input signals of the pixel drivers.

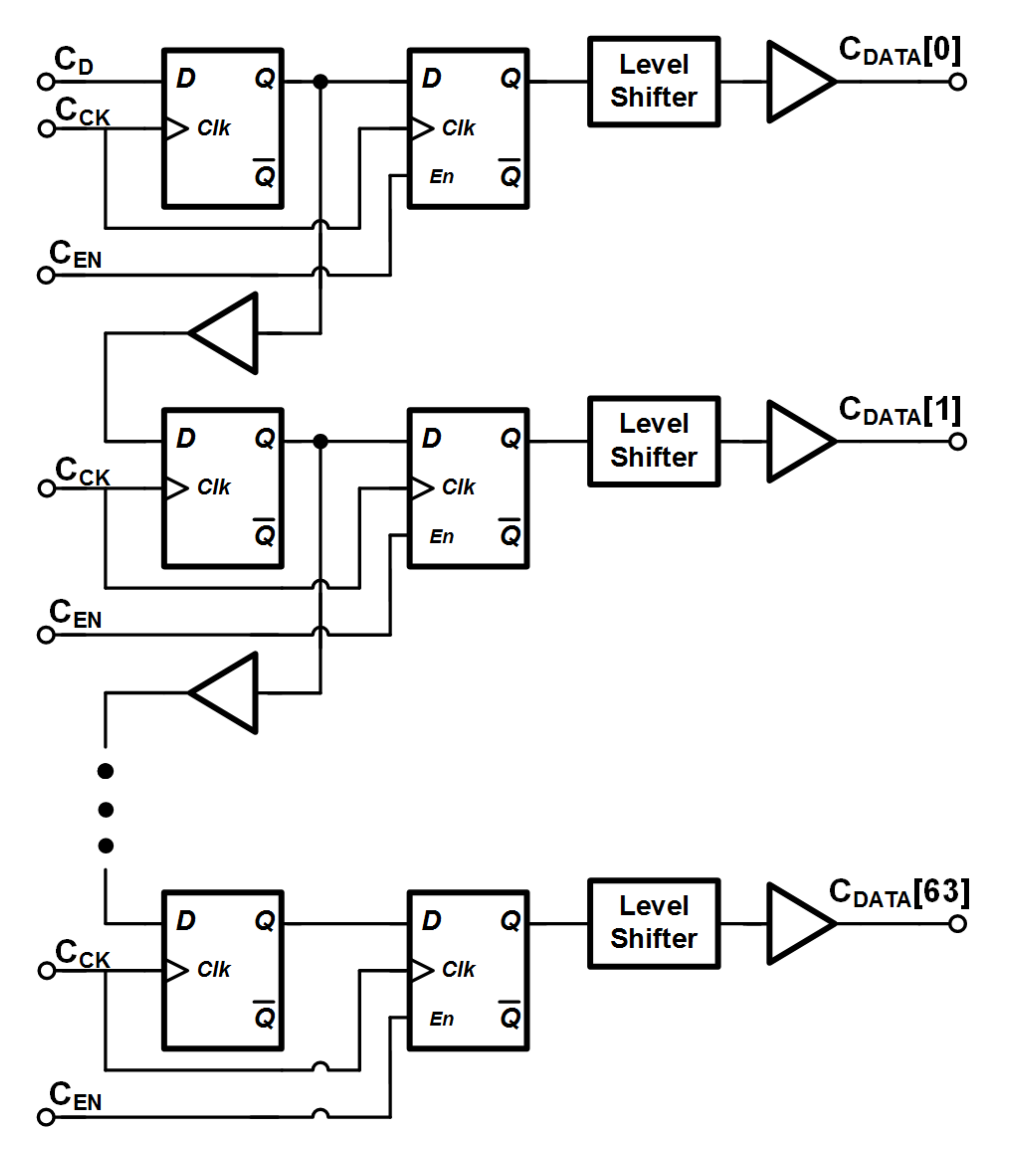


Figure 3.8 Diagram of column driver.

The timing of the column driver is shown in Figure 3.9. C_D continually sends the display data bit by bit. After 64-bit data, C_{EN} is enabled with logic '1'. Hence, 64-bit data is saved in $C_{DATA}[0] - [63]$. For example, in Figure 3.9, Data 63 is saved in $C_{DATA}[63]$, which is logic '1', and Data 0 is saved in $C_{DATA}[0]$ as logic '0'.

To support 36×64 pixel display, row-by-row progressive scanning is employed. In such scanning, one row is enabled at one time while column display data $C_{DATA}[0] - [63]$ is fed into the pixel drivers of that row, and the same procedure repeats for other rows. The complete timing for the written display data is described in the following section.

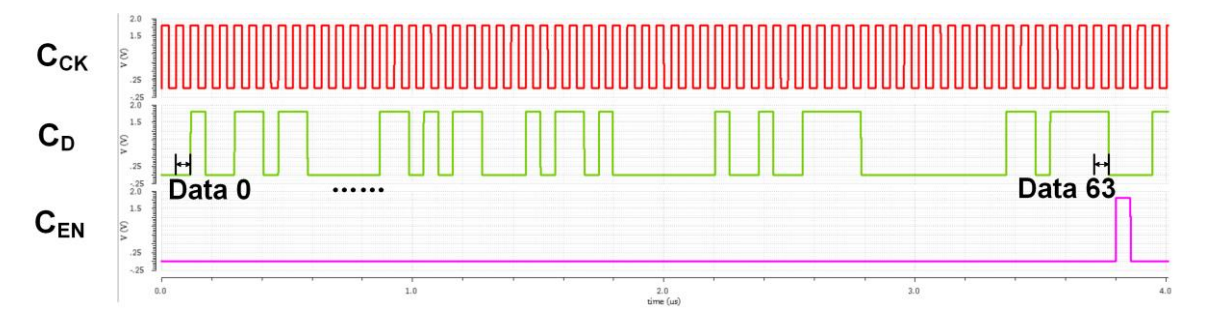


Figure 3.9 Timing of column driver.

3.4 Pixel Driver

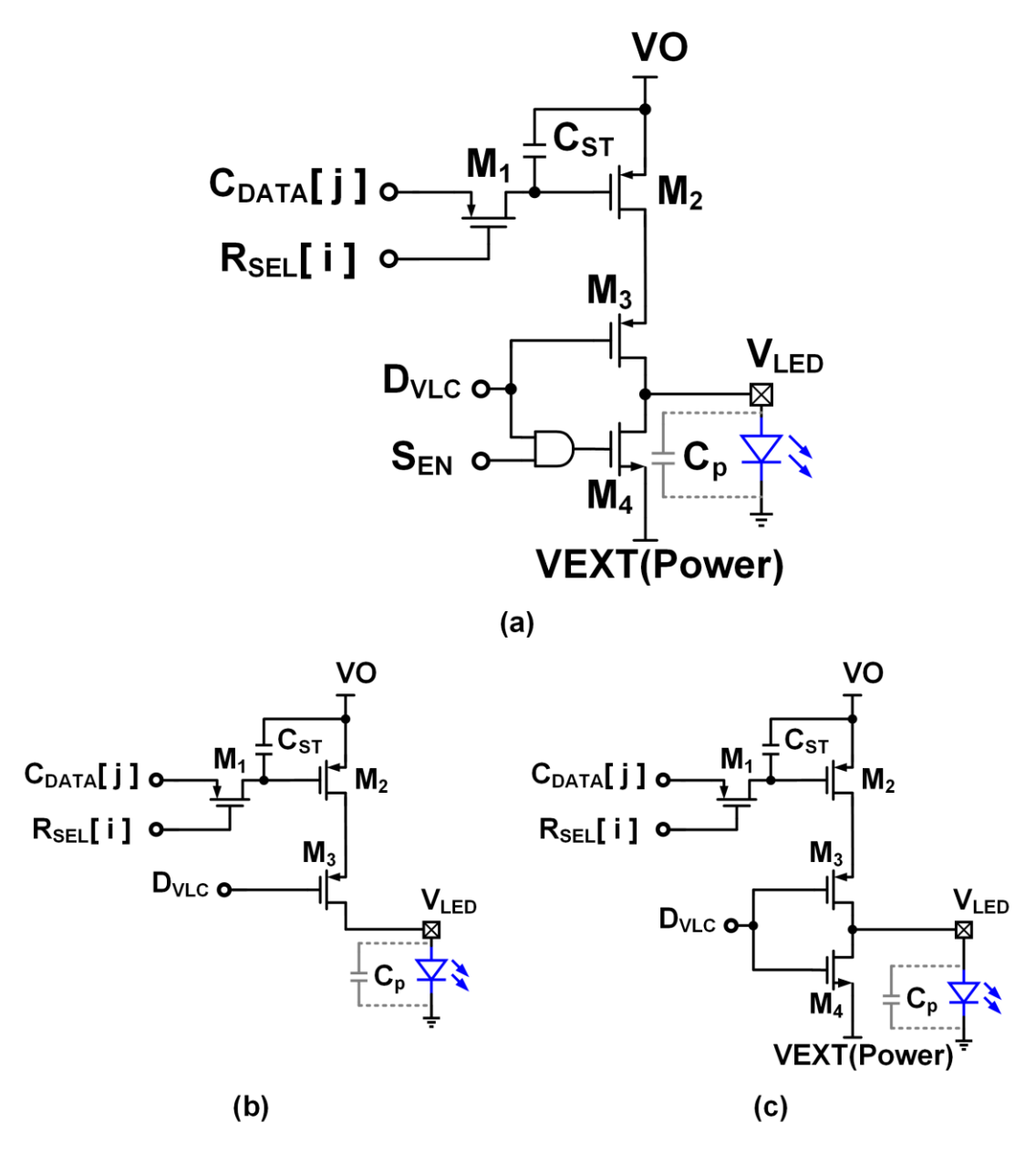


Figure 3.10 (a) Proposed pixel driver can operate in different modes by S_{EN} settings, (b) $S_{EN}='0'$, conventional mode, (c) $S_{EN}='1'$, proposed 2-driving-transistor mode.

The proposed pixel driver, supporting display and VLC simultaneously, is able to perform in different modes by S_{EN} settings, as shown in Figure 3.10. The driver of *Pixel(i,j)* consists of three PMOS transistors (M₁, M₂, M₃), an NMOS transistor (M₄), an AND logic gate and a capacitor C_{ST}. When R_{SEL}[i] is enabled (which means *Row i* is activated), M₁ is open and C_{ST} stores the display information of *Pixel(i,j)* from C_{DATA}[j]. After that, R_{SEL}[i] is disabled and the scanning of *Row i* is finished. After all pixels are loaded with the display data, the VLC data signal D_{VLC} is enabled to display the programmed image and transmit VLC data by modulating the light intensity of the micro-LEDs. When S_{EN} is set to digital '0', then the NMOS M₄ is turned off because its gate is controlled by digital '0', and the pixel driver works in the conventional mode with only one power supply and one driving transistor (M₃), as shown in Figure 3.10(b). In contrast, if the S_{EN} is digital '1', the gate of M₄ is actually connected to the D_{VLC}, and the pixel driver has two power supplies (VO and VEXT) and two driving transistors (M₃ and M₄), which is named 2-driving-transistor (2DT) mode, as shown in Figure 3.10(c). In both modes, the pixel driver is able to support display and VLC functions, while 2DT mode improves the bandwidth of micro-LEDs, which is discussed later.

3.4.1 Timing of Pixel Driver Array

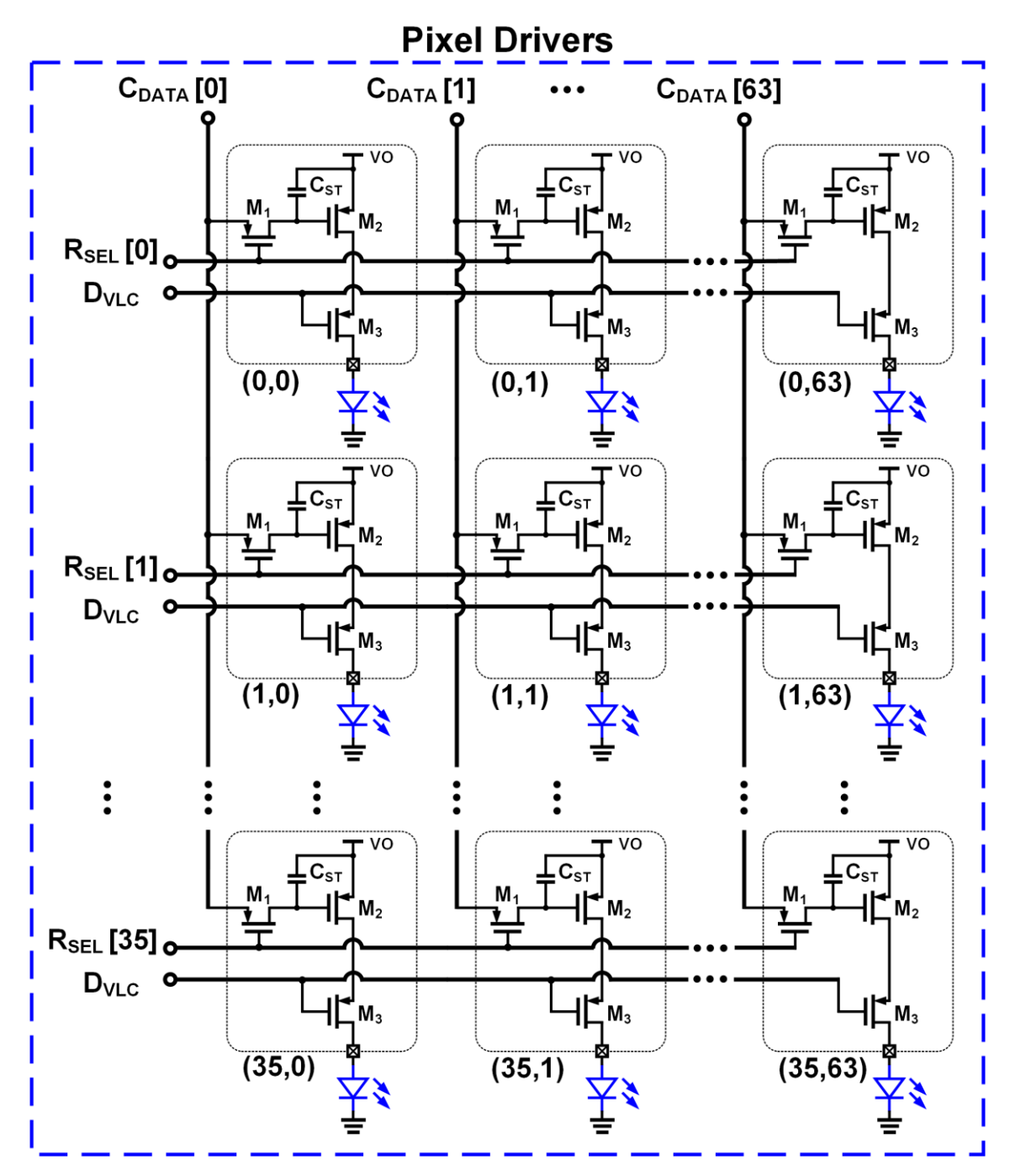


Figure 3.11 Structure of pixel driver array.

Figure 3.11 shows the structure of the 36×64 pixel drivers with flip-chip bonded micro-LEDs, in which the conventional mode unit pixel driver is used to simplify the diagram. The pixel driver array is controlled by 36 row selection signal lines R_{SEL} from the row driver, 64 column display data signal lines C_{DATA} from the column driver and a global VLC data signal D_{VLC} .

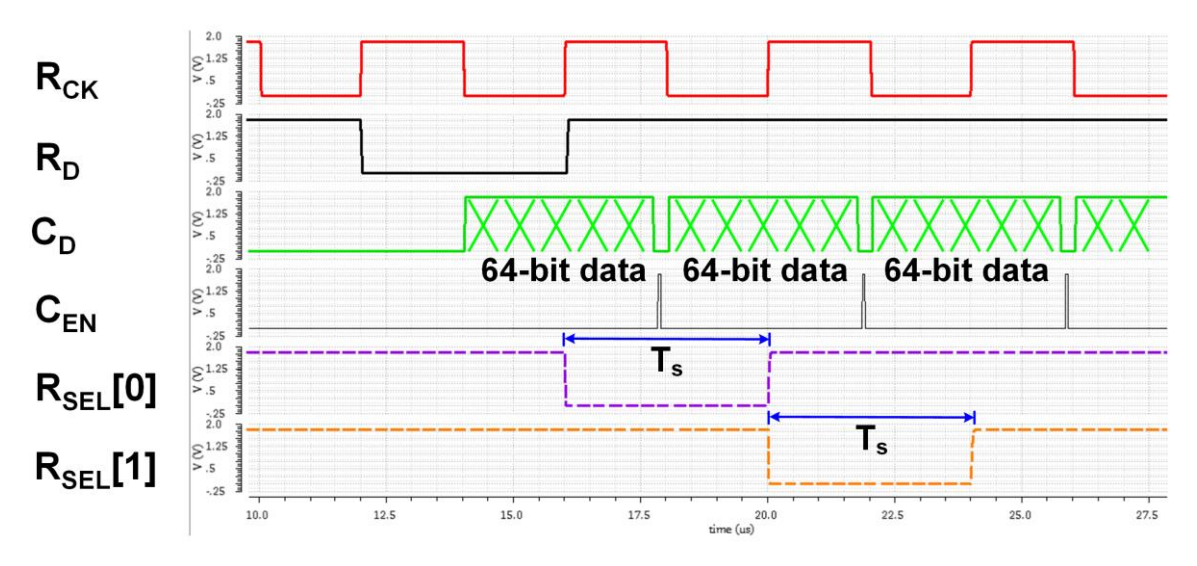


Figure 3.12 Timing of display data update.

The display data is updated through row-by-row progressive scanning, and the timing of the update is shown in Figure 3.12. First, the 64-bit display data of $Row\ 0$ is written into the column driver serially through C_D . Then, C_{EN} is enabled, and the 64-bit display data is loaded into the signal lines from $C_{DATA}[0]$ to $C_{DATA}[63]$. $R_{SEL}[0]$ is already in the enabled status, and each C_{ST} of $Row\ 0$ will store the display data from C_{DATA} . After that, $R_{SEL}[0]$ becomes disabled and the scanning of $Row\ 0$ is finished. The same procedure is then repeated for the other rows. After all pixels are loaded with the display information, D_{VLC} is enabled to display the programmed image and transmit VLC data.

3.4.2 Conventional Mode Pixel Driver

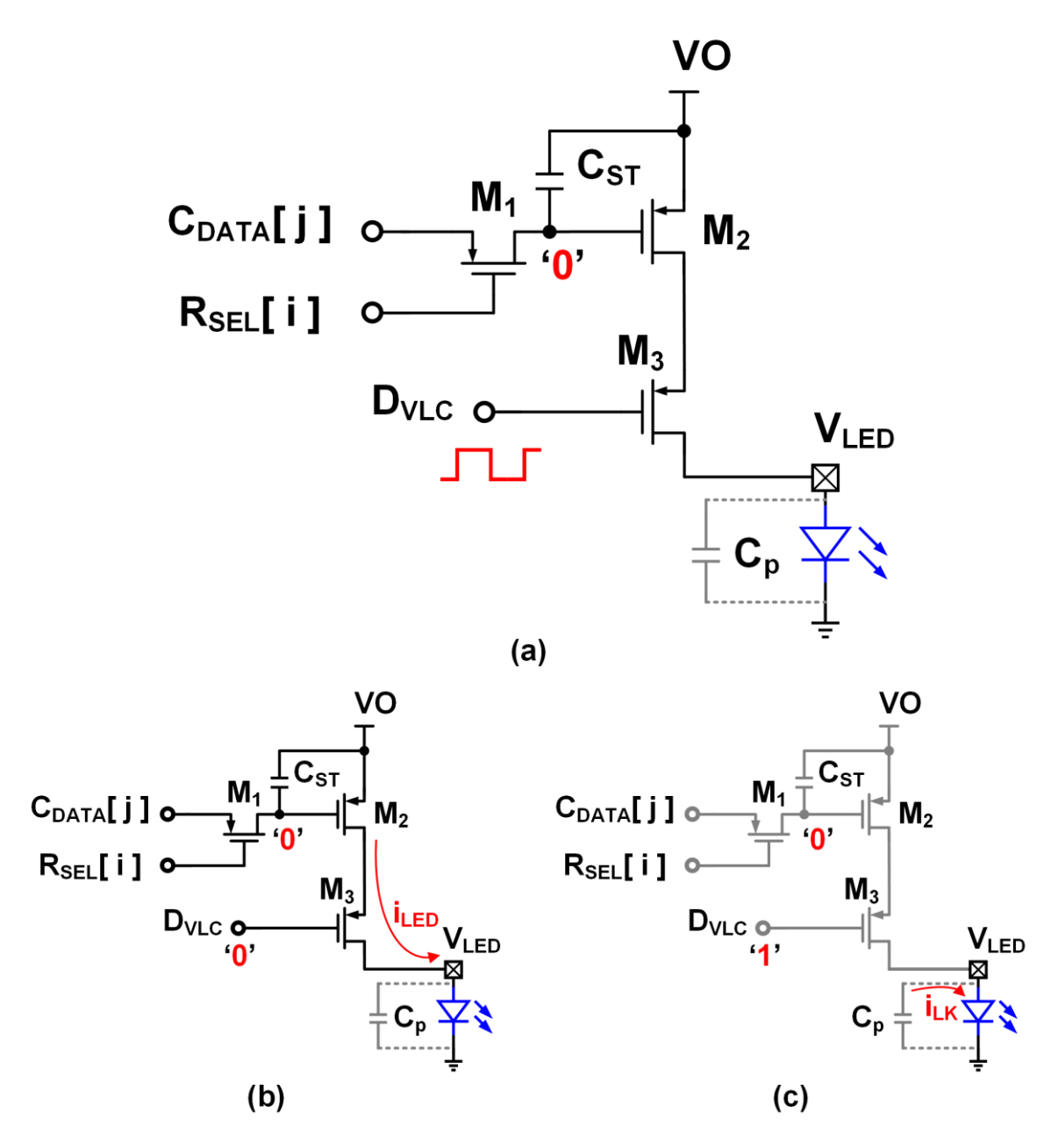


Figure 3.13 (a) Conventional mode pixel driver with '0' stored in C_{ST} and D_{VLC} input, (b) when D_{VLC} ='0', forward current i_{LED} charges the micro-LED, (c) when D_{VLC} ='1', leakage current i_{LK} flows through the micro-LED.

Only after C_{ST} stores the digital '0' and M_2 is turned on, the current through the micro-LED, which is proportional to the light intensity, be modulated by the incoming VLC data D_{VLC} , which is applied on the gate of M_3 . Figure 3.13(a) shows the conventional mode pixel driver with '0' stored in C_{ST} and D_{VLC} input.

When the coming data is digital '0' (D_{VLC}='0'), M₂ and M₃ are turned on, and the forward current i_{LED} charges the micro-LED from the power supply VO. Hence the voltage across the micro-LED will increase, as shown in Figure 3.13(b).

If the coming bit is digital '1' (D_{VLC} ='1'), M_3 turns off and cuts the forward current i_{LED}. However, due to the large parasitic capacitance C_p of the micro-LED, the voltage V_{LED} will decrease due to the leakage current i_{LK}. And i_{LK} also decreases following V_{LED} , as well as the light intensity of the micro-LEDs. Moreover, the lower level of V_{LED} is variable and highly dependent on the number of consecutive digital '1's in the incoming VLC data D_{VLC} . Consequently, the swing and the fall time of V_{LED} are input data-dependent, not a constant value, which affects the rise time of V_{LED} . Thus, the bandwidth of micro-LEDs driven by a conventional mode pixel driver is limited.

3.4.3 Proposed 2-Driving-Transistor Mode Pixel Driver

The 2DT mode pixel driver has two power supplies and two driving transistors for the micro-LED. Figure 3.14(a) shows the 2DT mode pixel driver with '0' stored in C_{ST} and D_{VLC} input.

When the coming data is digital '0' (D_{VLC}='0'), M₂ and M₃ turn on. The topology is the same as that in the conventional mode, and the forward current i_{LED} goes through M₂ and M₃ and charges the micro-LED, as shown in Figure 3.14(b).

If the coming bit is digital '1' (D_{VLC} ='1'), M_3 turns off while M_4 turns on. Then another power supply VEXT (<VO) can help sink the current i_s from C_p , as shown in Figure 3.14(c). V_{LED} will decrease faster than in the conventional mode pixel driver, with the help of current i_s and i_{LK} . After that, the power supply VEXT provides the forward current i_h to compensate for the charge loss on C_p due to the leakage current i_{LK} , and holds the lower level of V_{LED} at a constant value, as shown in Figure 3.14(d).

Consequently, in the 2DT mode pixel driver, the swing of V_{LED} is fixed, not data-dependent anymore, and the fall time of V_{LED} is reduced with the help of M_4 and VEXT. Moreover, the swing of V_{LED} can be reduced by tuning the value of VEXT, which helps to decrease the rise and fall time. Hence, the bandwidth of micro-LEDs in the 2DT mode pixel driver is expanded.

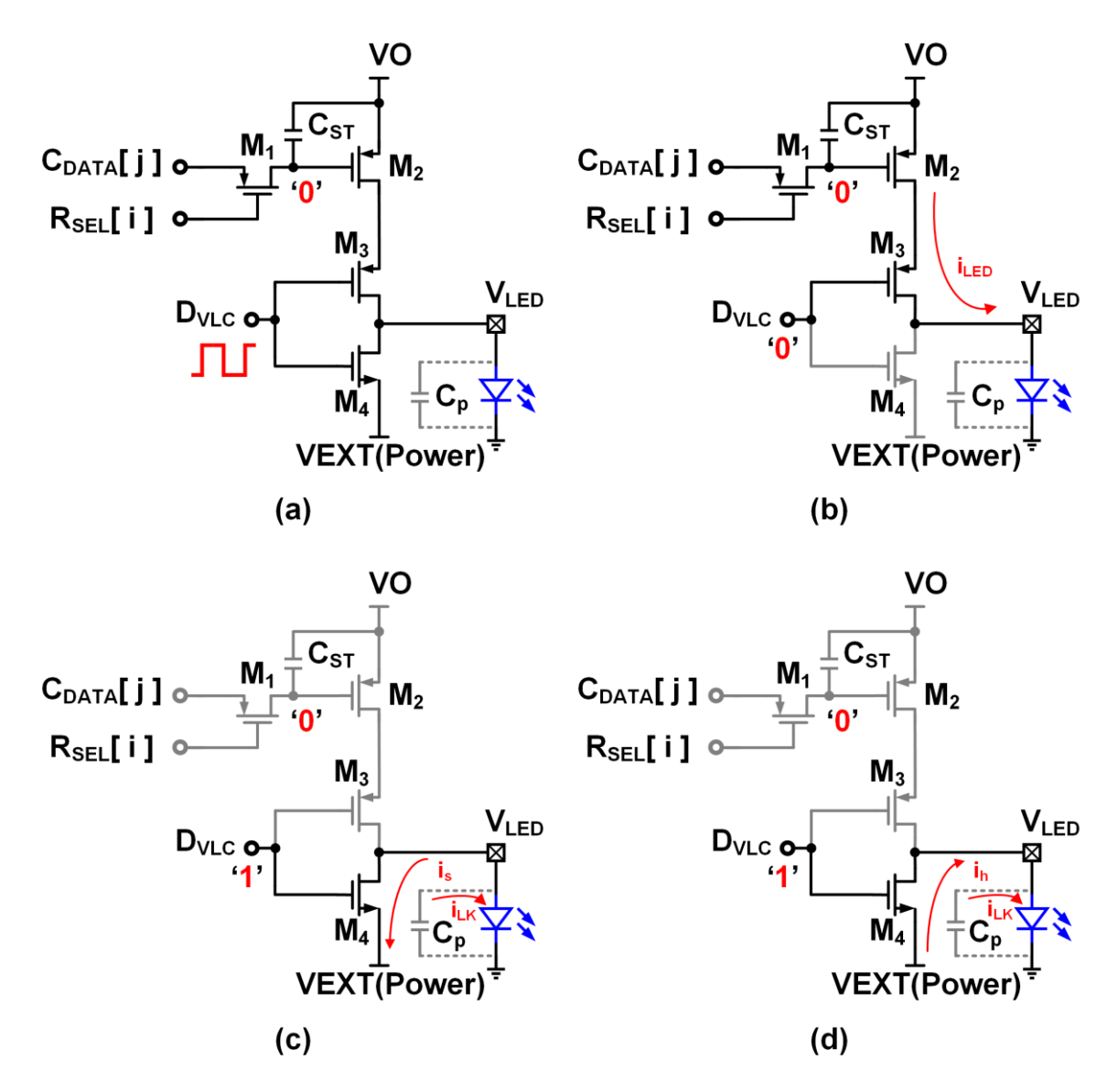


Figure 3.14 (a) 2DT mode pixel driver with '0' stored in C_{ST} and D_{VLC} input, (b) when D_{VLC} ='0', forward current i_{LED} charges the micro-LED, (c) when D_{VLC} ='1', power supply VEXT sinks the current i_s from C_p , (d) current i_h from VEXT compensates for the leakage current i_{LK} and maintains the value of V_{LED} .

3.5 Experiments and Results

The experimental VLC setup is shown in Figure 3.15. All pixels of the AMLED micro-display are turned on to get the highest light power [3.3]. The VLC signal is transmitted by the AMLED system from the baseband in TX FPGA, and received by an in-house-developed receiver (RX) on the receiver side. PRBS-7 pattern is used in the measurement.

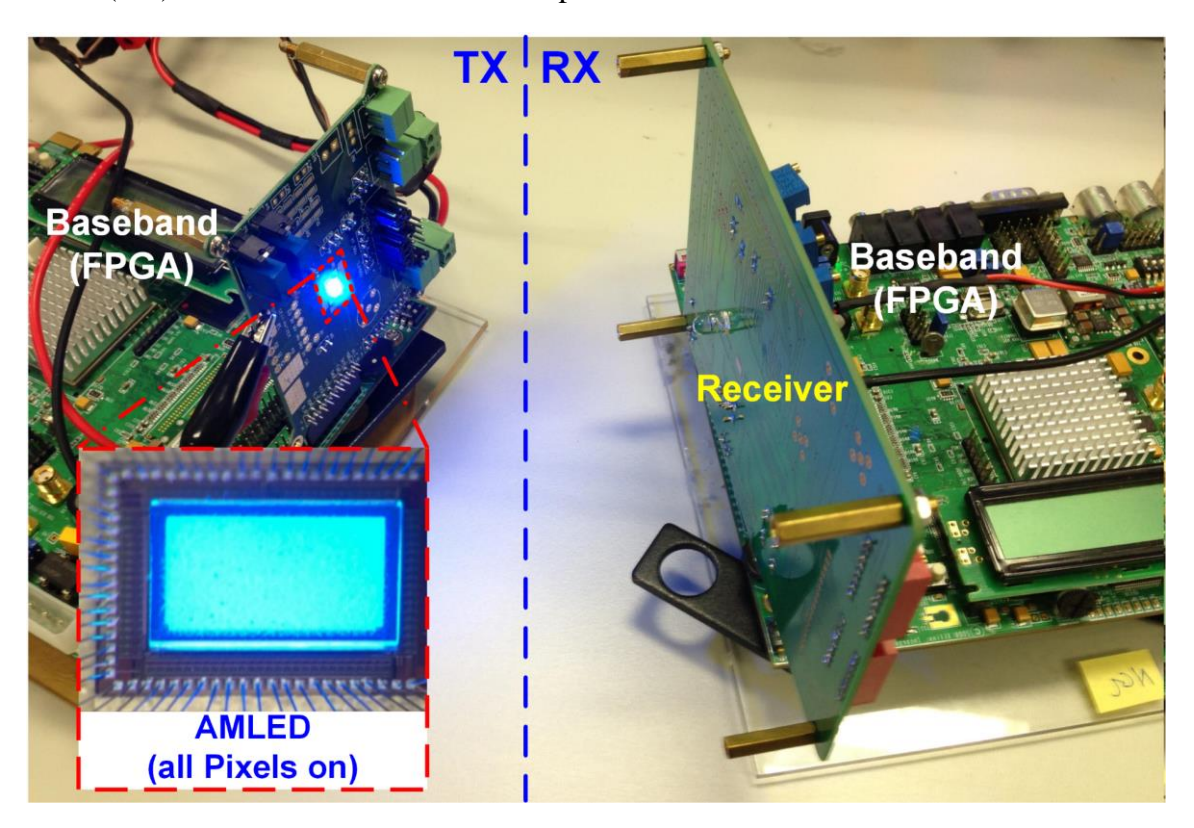


Figure 3.15 VLC experimental setup.

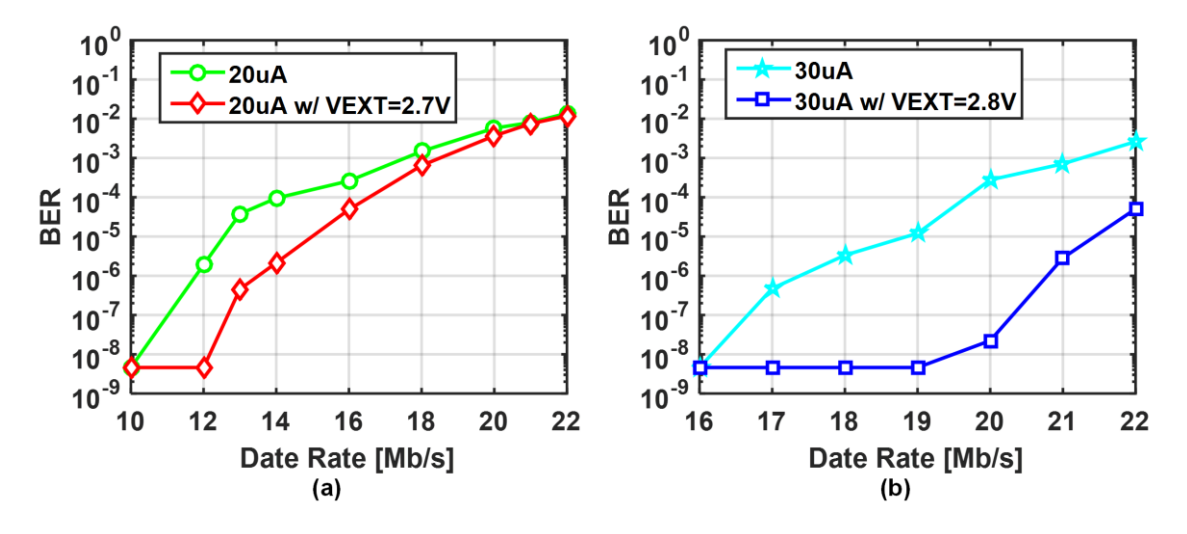


Figure 3.16 BER vs. data rate of conventional and 2DT mode pixel driver at 10 cm distance, (a) with 20 μA per pixel, (b) with 30 μA per pixel.

For all the BER measurement in this chapter, the number of collected bits is around 100 times larger than the reciprocal of the BER, except for the best BER of 4.6×10^{-9} , which has around 1 G collected bits to save the measurement time. For example, if the BER result is 10^{-7} , then collected bit number is around 1 G. While the measurement is performed under different data rates ranging from 10 Mb/s to 22 Mb/s. Then it takes around 62.5 seconds for the gen-2 AMLED to transmit 1 G bits at a 16 Mb/s date rate.

At 10 cm distance, with an average pixel current of 20 μ A and 30 μ A, the bit error rate (BER) results of the 2DT mode and conventional mode driver are shown in Figure 3.16. In Figure 3.16(a), compared with the conventional mode, the proposed 2DT mode pixel driver with VEXT=2.7 V, can improve the BER performance from 1.9×10^{-6} to 4.9×10^{-9} at a 12 Mb/s data rate with 20 μ A per pixel. To achieve a BER $< 10^{-5}$, the data rate is expanded from 12 Mb/s to 14 Mb/s by the proposed 2DT mode driver, with 16.7% improvement. However, the extra current of 4 μ A per pixel, is needed for the proposed 2DT mode driver. It consumes additional 19% power. And with 16% data rate improvement, the bit efficiency decreases by 1.9%.

In Figure 3.16(b), with 30 μ A per pixel, the BER performance is improved from 1.2×10⁻⁵ to 4.9×10⁻⁹ at a 19 Mb/s data rate by the 2DT mode driver. Moreover, to achieve a BER < 10⁻⁵, the data rate is expanded from 18 Mb/s to 21 Mb/s by the 2DT mode driver, with 16.7% improvement. Additional 21% power is consumed by the 2DT mode driver. Thus the bit efficiency reduces by 3.6%.

Based on the above results, it is affirmed that the 2DT mode pixel driver can extend the bandwidth of micro-LEDs and improve the VLC data rate.

If the average current through the micro-LED increases from 20 μ A to 30 μ A per pixel, as shown in Figure 3.16, under a 16 Mb/s data rate, even using the conventional mode driver, the BER performance is improved from 2.6×10^{-4} to 4.9×10^{-9} . To achieve a BER < 10^{-5} , the data rate is expanded from 12 Mb/s to 18 Mb/s by increasing the current density, with 50% improvement. For the 2DT mode driver, to achieve a BER < 10^{-5} , the data rate is expanded from 14 Mb/s to 21 Mb/s by increasing the average current from 20 μ A to 30 μ A per pixel, with 50% improvement. Consequently, it is affirmed that increasing current can help improve the bandwidth of micro-LEDs.

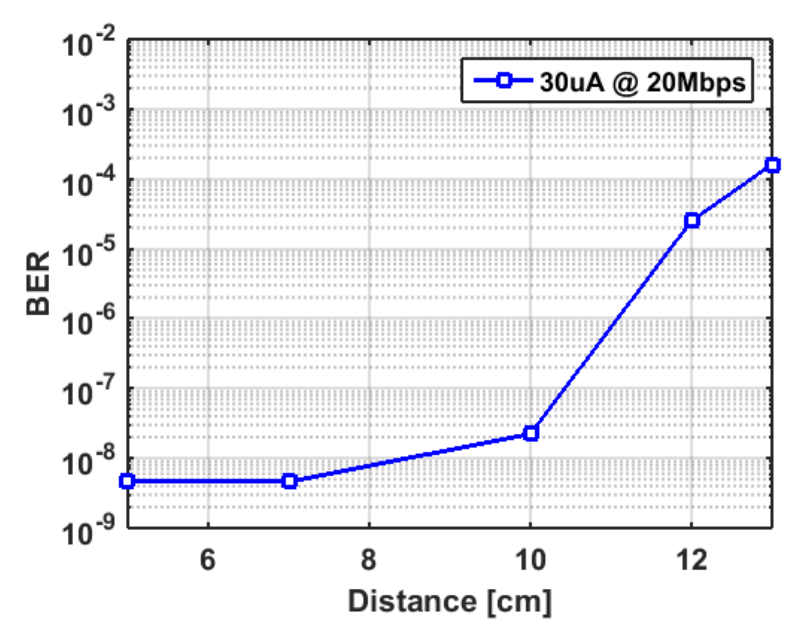


Figure 3.17 BER vs. distance of 2DT mode driver with 30 μA per pixel at 20 Mb/s data rate.

When the 2DT mode pixel driver modulates the micro-LED at a 20 Mb/s data rate, with an average current of 30 μ A per pixel, the BER results under different distances are shown in Figure 3.17. Due to the received light intensity drops with the increasing distance, the BER performance declines. To achieve a BER $< 10^{-4}$, the distance is up to 12 cm.

References

- [3.1] J. Jiang, L. Sun, X. Zhang, S. H. Yuen, X. Li, W.-H. Ki, C. P. Yue and K. M. Lau, "Fully-integrated AMLED micro display system with a hybrid voltage regulator," accepted for presentation at 2017 IEEE Asian Solid-State Circuits Conference (A-SSCC).
- [3.2] X. Li, L. Wu, Z. Liu, B. Hussain, W. C. Chong, K. M. Lau, and C. P. Yue. "Design and characterization of active matrix LED microdisplays with embedded visible light communication transmitter." *Journal of Lightwave Technology*, vol. 34, no. 14, pp. 3449–3457, 2016.
- [3.3] L. Sun, B. Hussain, X. Li, G. Zhu, and C. P. Yue, "A micro-LED driver with bandwidth expansion for visible light communications," accepted for presentation at *JSAP-OSA Joint Symposia* 2017.
- [3.4] M. Ershov, H. C. Liu, L. Li, M. Buchanan, Z. R. Wasilewski, and A. K. Jonscher, "Negative capacitance effect in semiconductor devices." *IEEE Transactions on Electron Devices*, 45, no. 10 (1998): 2196-2206.

CHAPTER 4 CONCLUSION AND FUTURE WORK

4.1 Conclusion

Visible light communication (VLC) using LEDs has recently attracted a great deal of research interest for Light-Fidelity (Li-Fi) applications. This thesis presents two Adaptive Threshold Decoding (ATD) algorithms for Li-Fi data recovery and an AMLED micro-display driver with bandwidth expansion techniques, for simultaneous display and VLC (SD-VLC) applications.

The conventional Constant Threshold Decoding algorithm cannot handle the VLC data recovery in SD-VLC, due to the varying received signal strength caused by changes in the displayed images or videos. The proposed Preamble-based ATD algorithm is able to recognize the VLC-enabled periods and calculate the threshold values by averaging the preamble sequence at the beginning of each data period. The Section-based ATD algorithm, on the other hand, recognizes the VLC-enabled period with the same method as the Preamble-based ATD, and averages the signal in each section to compute the corresponding threshold values. The measured BER of data received from a 4-frame/s micro-LED display is improved from 6.9×10^{-2} to 4.4×10^{-4} using the Preamble-based ATD algorithm compared to the conventional Constant Threshold Decision scheme, which is further improved to 3.6×10^{-4} by using Section-based ATD. However, the Section-based ATD algorithm requires larger computation and power.

A second-generation AMLED micro-display driver, consisting of a row driver, a column driver and proposed pixel drivers, is flip-chip bonded with a GaN micro-LED array with 36×64 pixels, each measuring $40\times40~\mu\text{m}^2$, as a transmitter for SD-VLC applications. The proposed pixel driver can extend the bandwidth of micro-LEDs, and improve the Li-Fi data rate, by fixing the lower level of the swing and increasing the driving current of the micro-LEDs. Implemented in a 0.18- μ m CMOS process, the AMLED micro-display with the proposed pixel driver can achieve a 20 Mb/s bit rate at 10 cm without lenses, which is four times as large as the 5 Mb/s modulation bit rate in the first generation.

4.2 Future Work

In simultaneous display and VLC applications, a control scheme and a new VLC date packet format are needed in the future to achieve better BER performance and good robustness in a practical system. The control scheme can dynamically enable and disable the VLC data transmission based on the displayed content on the transmitter side, and control the gain of variable-gain amplifier (VGA) on the receiver side to achieve automatic gain control (AGC). The overall brightness of the next frame or $Frame\ N+1$, which is in proportion to the corresponding VLC signal amplitude of $Frame\ N+1$, is encoded into the preamble or header in the VLC date packet of this frame or $Frame\ N$. The encoded information is received and used to control the gain of VGA, which is necessary for any wireless communication systems, to amplify the received VLC signal of $Frame\ N+1$. Thus, automatic gain control (AGC) is achieved. Together with the AGC and proposed ATD algorithms, the received VLC data can be recovered better. Furthermore, it provides good robustness for the practical system. If the overall brightness of the $Frame\ N+1$ is too small for reliable VLC data transmission, then the VLC function should be disabled during the next frame ($Frame\ N+1$) on the transmitter side.

For the micro-display system, further investigation of the micro-LED model, including electrical and optical characteristics, is critical for the micro-LED driver design to further improve the data rate and bit efficiency.

PUBLICATIONS

- [1] **Liusheng Sun**, Xianbo Li, Babar Hussain, and C. Patrick Yue, "An adaptive threshold decoding algorithm for visible light communication data recovery from LED-based display systems," in 2017 IEEE Photonics Conference (IPC), accepted.
- [2] **Liusheng Sun**, Babar Hussain, Xianbo Li, Guang Zhu, and C. Patrick Yue, "A micro-LED driver with bandwidth expansion for visible light communications," in *JSAP-OSA Joint Symposia 2017*, accepted.
- [3] Junmin Jiang, **Liusheng Sun**, Xu Zhang, Shing Hin Yuen, Xianbo Li, Wing-Hung Ki, C. Patrick Yue and Kei May Lau, "Fully-integrated AMLED micro display system with a hybrid voltage regulator," in *2017 IEEE Asian Solid-State Circuits Conference*, accepted.